FINAL REPORT

GAS FLOW IN WELLS AFTER CEMENTING

Andrew K. Wojtanowicz, Wojtek Manowski, and Somei Nishikawa
Louisiana State University

Submitted to:

US Department of Interior
Minerals Management Service
381 Elden Street
Herndon, Virginia 20170-4817

Baton Rouge, Louisiana
September 5, 2000

TABLE OF CONTENTS

EXECUTIVE SUMMARY

The subject of this work concerns early annular flow of gas after cementing. The phenomenon is potentially dangerous because it could evolve into either breaching of gas to the surface - resulting in a blowout, or inter-zonal communication - resulting in fracturing weaker formations, underground blowout, or cratering.

The structure of this work reflects a systematic analysis of the problem of flow after cementing. First, it presents the analysis and documentation of available data from case histories occurring on the US Outer Continental Shelf and the 200-mile Exclusive Economic Zone and other similar offshore areas. Data from these areas have been accumulated during the last twenty years. Field case histories are supplemented here with analysis of field experiments pertaining to the two major phenomena controlling the flow after cementing: hydrostatic pressure loss and volumetric reduction of cement caused by downhole filtration.

In view of limited available data, analysis of field cases of flow after cementing has been limited to qualitative circumstantial observations regarding common features of the affected wells such as: Casing strings are typically set at shallow depths; Hole sizes are relatively large; and; Cement slurries are displaced to the surface. Neither of these features, however, could be considered uniquely associated with gas flow as has been shown by comparing "non-flowing" and "flowing" wells.

No specific property of cement or well has been found that could be related to the incidents of flow after cementing. Based on available cement data (density, and volume) it is not possible to identify anomalous properties of cement slurries that would make wells flowing. In fact, it makes more sense to assume that these cements were typical standard slurries. Also, there is no evidence that BOP/diverter nipple-down operation could be a factor in the phenomenon. Thus, we conclude that incidents of flow after cementing are statistical events caused by the presence of shallow gas pockets tapped by the wells. The pockets may go undetected while drilling the well if their pressure gradients are below equivalent pressure gradients of drilling fluid.

Second, a review of the present understanding of the phenomena governing flow after cementing is presented. Particularly important here is the analysis of mathematical models that have been used to describe the mechanism of hydrostatic pressure loss in cement during the dormant and transition stages of slurry setting. The review shows lack of consistent theory and emphasis on friction (SGS) effect in modeling the pressure loss phenomenon. The effect of cement (annular) compressibility has been considered by some researchers in static rather than dynamic (transient flow) manner.

In addition to the review of published models a new model of pressure unloading is proposed and verified with the field data. The model considers initial propagation of pressure transient upwards the cement column from the depth of fluid loss into the rock. The model has been validated using data from the field test with pressure gauges installed in the cemented annulus. Bottomhole pressure calculated from the model showed the initial rapid reduction measured in the test well.

The pressure-unloading model was used in a sensitivity study to identify parameters controlling pressure loss in cement and intrusion of gas. The study revealed that large annuli with high water loss would give rapid and large reduction of hydrostatic pressure in the cement column and more likely intrusion of gas. The observation implies that surface holes should be

more sensitive to gas migration than deep holes. Also, cement slurry filtration should be minimized in surface holes.

The sensitivity study also showed that annular cement systems having large compressibility would be more tolerant to fluid loss in terms of losing hydrostatics than the low-compressibility systems. The observation emphasizes the importance of determining the annular system compressibility involving the open-hole lithology. Further studies are needed to develop practical methods for evaluation of annular compressibility.

Third, presented here is a survey and documentation of current technology for preventing gas flow after cementing surface casing in offshore operations. The state-of-the-art in methods to prevent and combat the problem follows. Also included is a survey and documentation of current operator policy and procedures for handling gas flow after cementing surface casing in offshore operations.

The survey of field practices showed that the main challenge for operators is to identify the area with gas migration problem serious enough to justify investment in preventive technology. Statistical nature if the phenomenon makes operators willing to take a risk rather than to spend money on prevention; Operating companies avoid using special cements on a routine basis due to their high cost.

The last part of this report concerns analytical methods for prediction of the hazards of flow after cementing. Analyzed are various indicators of the hazards, their physical background, and calculation procedures. The predictive power of the indicators has been statistically evaluated by comparing two clusters of wells, both with and without the gas migration problem. No significant correlation has been discovered.

Also proposed in this report is a new method for post-cementing flow risk evaluation based upon mathematical modeling of pressure and computing time-to-underbalance (TTU), i.e., conditions for formation fluid inflow into the cement slurry and the beginning of flow. In the method, theoretical time of hydrostatic pressure reduction down to the gas zone pressure value is calculated and used as a relative estimator of risk; the shorter the TTU value the higher the risk becomes. The method has been statistically validated by seeking a correlation between TTU and actual time of gas flow on the surface recorded in the flowing wells. Two models were used to calculate TTU, cement gellation model (conventional), and the pressure-unloading model.

For the gellation model, the correlation was weak mostly due to insensitivity of TTU to the well conditions. As the model is entirely controlled by SGS, and slurries used in the wells were similar calculated TTU gives almost identical values independent from depth.

For the pressure unloading model the correlation was also weak but the calculated values of TTU were much smaller and varied significantly. Thus, this model should be considered for further work on indexing the gas flow risk assessment.

1. FIELD EVIDENCE OF FLOW AFTER CEMENTING

Several accidents in wells on the Outer Continental Shelf (OCS) have occurred shortly after cementing while rig personnel waited for cement to set. In all these events, the diverter system was not completely nippled down before the cement developed sufficient compressive strength. Typically, a few hours after cement placement, a well would start flowing gas. Flow of this type is difficult to control and—if not eliminated—may cause loss of well integrity, spillage, or blow-out. The problem is known as "early gas migration," or "shallow gas flow."

1.1 Field Case Histories of Flow after Cementing

From 1965 through 1994, sixteen cases of early flow after cementing were recorded in the Gulf of Mexico, as shown in Table 1.1 and Appendix A. The average flowing time was 4.6 hours after cement placement. Several wells exhibited the problem at the same time that the displacement of the cement slurry was completed. Depths of these wells averaged 3,412 ft; a well over 5,000 ft was a rare case. The casing sizes (surface casings or intermediate casings) ranged from 10.75 in. to 20 in.. Fourteen wells were cemented to the surface.

Table 1. Flowing Wells in the Gulf of Mexico

No.	Date	Rig Type	Area	Previous Casing Shoe (ft)	Casing Shoe Depth (TVD, ft)	Start Nipple Down (hours)	Surface Flow Started after (hours)
1	9/16/65	Platform	SM	322	2,698	-	0
2	12/14/72	Platform	SS	632	2,501	?	?
3	10/1/75	Drill Ship	EI	1,104	4,088	?	?
4	3/15/76	Platform	EI	1,035	2,716	5.5	5.5
5	7/6/77	Drill Ship	SM	800	4,707	5	10.5
6	2/14/78	Jackup	MI	1,000	2,000	-	3.5
7	6/1/79	Drill Ship	WD	979	3,500	-	1.0
8	5/26/83	Jackup	MC	1,933	4,120	-	0
9	10/21/83	Jackup	GI	1,243	3,991	-	5.5
10	1/8/89	Jackup	MP	1,335	1,386	0.3	2.3
11	5/8/91	Jackup	BA	1,000	3,940	?	?
12	11/22/92	Jackup	EI	1,105	4,780	7.0	8.0
13	2/25/93	Jackup	MP	530	826	4.5	7.0
14	4/18/93	Jackup	SS	1,013	4,550	4.0	6.0
15	3/27/94	Jackup	PN	1,000	5,462	1.5	2.5
16	7/19/94	Jackup	ST	1,414	3,326	-	5.5
				Average value	3,412		4.6

Three features were common for all these events:

- Casing strings were set at shallow depths;
- Hole sizes were relatively large;
- Cement slurries were displaced to the surface.

A typical sequence of events leading to flow after cementing can be summarized in the following steps:

1. Cement is pumped and displaced successfully; the job appears to proceed without problems.
2. After a few hours of WOC, the diverter/BOP stack is nippled down and the well starts to flow.
3. The diverter is nippled up again; the well is diverted in an attempt to control the flow.
4. Even if the diverter does not fail, the well is flowing and is becoming more and more and difficult to control.
5. Various means of restoring control over the well are attempted, e.g., circulating heavy mud through tubing into the annulus, diverting the well, closing the well.
6. In case of severe flow, the rig is evacuated.
7. Sometimes the well can bridge after a few hours/days.
8. If the well is salvaged, it is thanks more to favorable circumstances than successful operation.

1.2 Field Experiments

Early gas migration is considered to result from the hydrostatic pressure loss in the cement slurry during the transient-gellation period. Static gel strength (SGS) development associated with the downward movement of the slurry caused by fluid loss and chemical shrinkage is generally cited as the cause of the hydrostatic pressure loss. Once the hydrostatic pressure at a gas-zone becomes underbalanced gas invades the cement in the annulus and the flow begins.

1.2.1 Hydrostatic pressure loss experiments

Cooke, et al. (1983) published experimental results of downhole pressure after primary cementing using full-scale wells to investigate causes of gas migration behind the casing. Fig. 1 shows one of these experiments to measure the downhole pressure. Six sensors were attached at various depths on the casing and pressure and temperature were recorded. Fig. 2 represents the result of the hydrostatic pressure loss. The hole size was 7 7/8 in. and 2 7/8-in. casing was run to a depth of 8,900 ft. Nearly 400 bbl of 16.6-ppg cement slurry was pumped. The density of drilling mud was 10.2 ppg. The hydrostatic pressure dropped rapidly soon after cementing and altered at a slower rate with time.

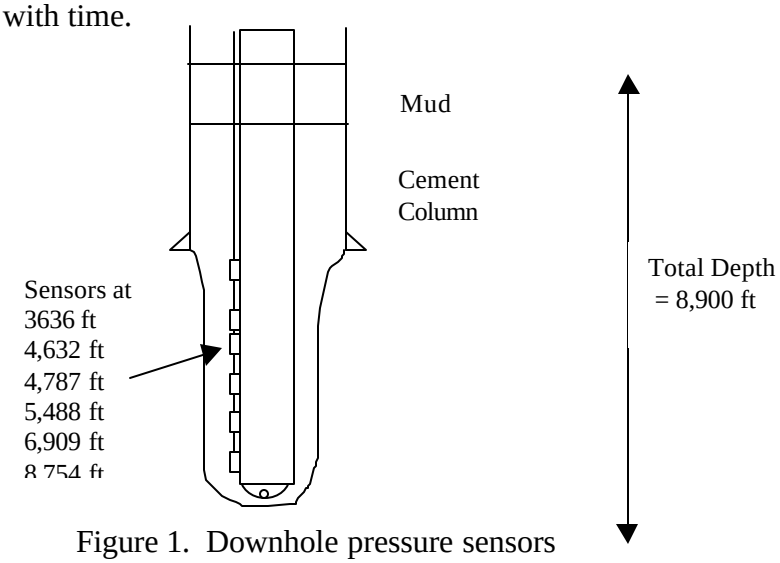

Figure 1. Downhole pressure sensors

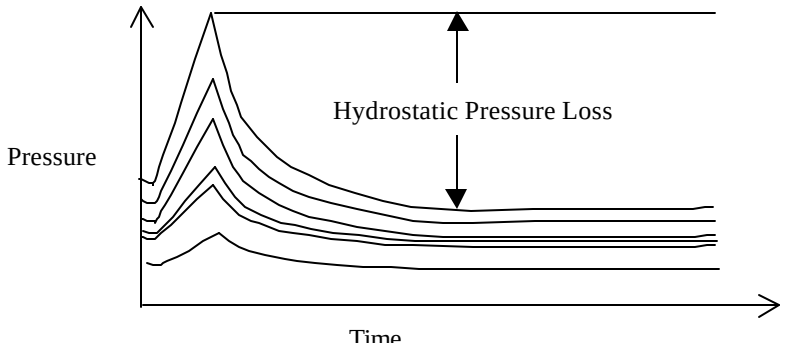

Figure 2. Hydrostatic pressure loss

Table 2 shows the hydrostatic pressure loss in the data of this experiment. Almost 3,000-psi pressure drop was observed at a depth of 8,754 ft.

Table 2. Hydrostatic Pressure Loss in Well Cement After Placement

Depth (ft)	Pressure Immediately after Placement (psi)	Pressure 360 min after Placement (psi)	Pressure Loss (psi)
3,636	2,600	1,700	900
4,632	3,400	2,050	1,350
4,787	3,550	2,300	1,250
5,488	4,200	2,550	1,620
6,909	5,450	3,150	2,300
8,754	7,100	4,150	2,950

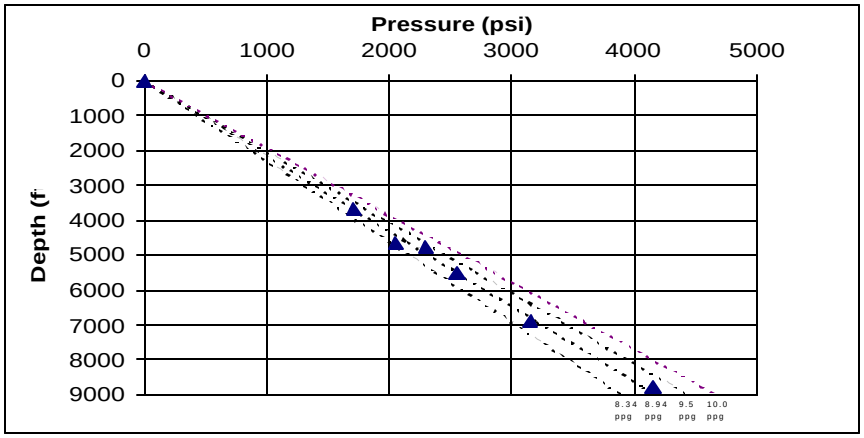

Figure 3. Hydrostatic pressure in annulus six hours after cement placement.

Fig. 3 shows the recorded hydrostatic pressures six hours after cement placement and illustrates that plots are placed on the pressure gradients between water and brine. Each sensor indicated that the hydrostatic pressure in the annulus converged to the normal formation-pressure gradient. This result is used for an assumption of the pressure-transient model.

On the other hand, a cement top was calculated at 1,200 ft from the rotary table using the density and a recorded hydrostatic pressure of the cement slurry after pumping the cement slurry was halted. After setting, the cement top was confirmed at a depth of 1,500 ft by the temperature log. The cement level was dropped 300 ft.

The hydrostatic pressure loss due to 300 ft gives $0.052 \times 16.6 \times 300 = 259$ psi. The sensor at bottom indicated 2,950 psi of pressure loss. Less than a 10% pressure loss was provided by the hydrostatic head loss.

1.2.2 Downhole Fluid Loss Experiments

Following the experiments of the hydrostatic pressure loss, the first attempt at downhole fluid-loss measurements was conducted for a series of four wells. Haberman, et al. (1992) published field experiments designed to investigate the downhole fluid loss. The experiments were conducted on four wells in the Mississippi River Delta.

In these experiments, the total depths (TD) were about 10,000 ft (Fig. 2.4). A large percentage of the formations drilled in each well were permeable sand. Log data for permeability were available and showed that about 70% of the surface area of the open-hole wall had permeability exceeding 1 md.

The depth of the surface casing was 2,500 ft, leaving 7,500 ft of the open hole during these tests. This open-hole interval was used for fluid-loss tests. The annulus was cemented from a depth of 5,000 ft to the bottom. The drilling fluid was left in the annulus from the cement top to the surface.

The volume of the downhole fluid loss was measured by closing in the casing annulus with the annular blowout preventer and pumping water into the annulus through the surface casing valves. An attempt was made to determine the accuracy of the measurements between the downhole fluid loss measured by the pressure-decline method and by the fluid-injection method.

To determine the effect of cement placement on the mud cake, the fluid loss before cementing was compared with the fluid loss after cementing. Then the effect of fluid-loss control additives was investigated.

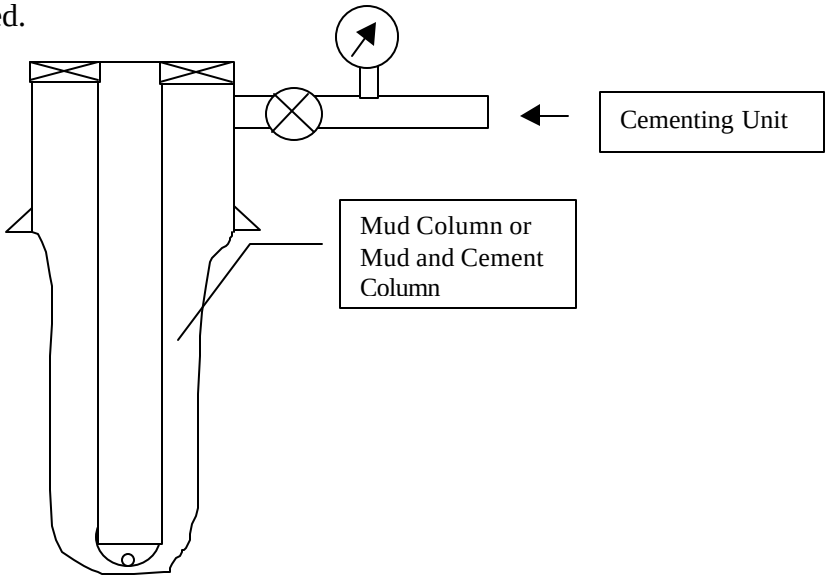

Figure 4. Well configuration for cement fluid loss experiment

In this investigation, characteristics of the fluid-loss in the field were:

- the drilling mud was 5 to 10 times lower than the API fluid-loss test;
- the cement slurry with fluid-loss additives was 100 to 200 times lower than the API cement fluid-loss test; and
- the cement slurry without fluid-loss additives was over 1,000 times lower than the API cement fluid-loss test.

The most remarkable point Haberman, et al., investigated was that the fluid-loss rate would be constant as a function of time over the relatively short time intervals. This result contradicts the conventional laboratory tests, which conclude that a fluid loss decreases with the square root. The researchers surmised that this result is due to the variations of pressure and temperature with depth in the well.

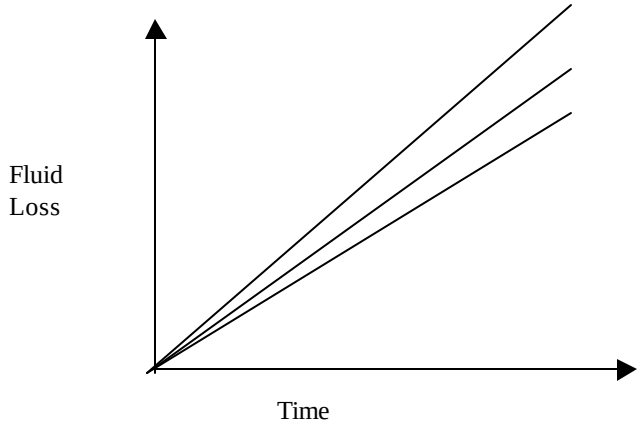

Figure 5. Pattern of fluid loss from cement slurry downhole

They reported that the presence of fluid-loss control additives in cement slurries had no effect on the fluid loss after cementing. The fluid loss did not alter substantially, although the casing was reciprocated. This indicated that the mud cake was not removed or altered by the cementing process. The fluid loss was controlled by the filtration properties of the mud cake.

Also, they concluded that the magnitude of the downhole fluid loss was equivalent to low-pressure API drilling-mud fluid loss of approximately 1 cm^3/30 min when the open hole was normalized to the same surface area as the API test.

2. MECHANISM OF PRESSURE LOSS IN CEMENT COLUMN

The reduction of volume of the hydrating cement slurry can be separated into bulk volume reduction and internal volume reduction. Bulk volume reduction is the decrease of outside dimensions of the slurry. Internal volume reduction does not affect cement outside dimensions, but the void space in the cement body increases. Cement bulk volume reduction is caused by the loss of filtrate into the permeable formations and by the chemical reactions occurring in hydrating cement.

Dynamic filtration during cement pumping does not lead to a loss of hydrostatic pressure. We will limit ourselves, thus, to the case of static filtration during cement hydration. Darcy law describes the phenomenon of static filtration in the case of a constant-thickness mud and cement cake. Flow rate of the fluid filtrating through the cake is:

$$q = \frac{A}{m} \cdot \frac{\Delta P}{\frac{e_c}{k_c} + \frac{e_m}{k_m}} \quad \text{.....} \quad \text{...(1)}$$

where:

A – cake area of flow, m^2

m – water viscosity, Pa - s

k_c – cement cake permeability, m^2

k_m – mud cake permeability, m^2

ΔP – pressure differential across cement and mud cake, Pa.

e_c- cement cake thickness, m

e_m- mud cake thickness, m.

Equation (1) is of limited use since it is often very difficult to estimate both cement and mud cake thickness and permeability. In the presence of a growing thickness of the cement cake due to the progression of filtration, equation (1) can be integrated to yield:

$$V_{fl} = \frac{\sqrt{\left(\mu \cdot \frac{e_m}{k_m}\right)^2 + 2 \cdot \frac{\mu \cdot R}{k_c} \cdot \Delta P \cdot t} - \mu \cdot \frac{e_m}{k_m}}{\frac{\mu \cdot R}{k_c \cdot A}} \quad \text{.....} \quad (2)$$

where:

V_{fl} – volume of filtrate, m^3

R - cake to filtrate volume ratio, d'less

t – time, sec.

Some parameters in eq. (2) can be obtained experimentally. A problem arises, however, when permeabilities need to be estimated, because cement permeability is a function of hydration, thus a function of time.

Both Sutton, et al. (1990) and Appleby and Wilson (1996) studied cement permeability. Sutton, et al., used a U-tube filled with cement and water on top. The researchers pressurized one leg of the tube to 5 psi and constantly withdrew water from the other. The rate of the withdrawal was measured while constantly monitoring pressure differential between the top of the legs. Cement permeability was computed using the Darcy equation:

$$k = \frac{q_{\max} \cdot \mu \cdot D}{4 \cdot A \cdot SGS} \quad \text{.....} \quad (3)$$

where:

$q_{\max}$ maximum flow rate, m^3/sec

m fluid viscosity, Pa-s

D diameter of the tube, m

A cross sectional area of the tube, m^2
SGS static gel strength of the cement in the tube, Pa.

According to Sutton, monitoring SGS development and permeability at the same time using this procedure is valid. The researchers found a strong relationship between slurry permeability and API fluid loss. In the study, early cement permeability ranged from 1000 md to 5 md.

Appleby and Wilson measured setting cement permeability in two different ways. The researchers observed that hydration causes suction, making any free fluid on the top of cement flow into cement body. They represented the mechanism driving water into shrinking cement as an effective sink rate. Sink rate is not, however, equal to the amount of water consumed by chemical reactions; rather, it corresponds to volume reduction due to a gain in density. Cement was modeled as a poroelastic body. The researchers obtained a relationship between rate of pressure decline and rate of strain change as a function of the sink term, which is expressed as:

$$\frac{\partial p}{\partial t} = \frac{K}{1+\frac{\phi \cdot K}{K_f}} \cdot \gamma \quad \text{..... (4)}$$

where:

p – pore pressure, Pa
t – time, sec
K – drained bulk modulus,
K_f – fluid bulk modulus,
f – porosity, d'less
g – sink rate , s^{-1}.

and as:

$$\frac{\partial \varepsilon_{kk}}{\partial t}\left(\approx \frac{1}{V_o} \cdot \frac{\partial V}{\partial t}\right) = \frac{1}{1+\frac{\phi \cdot K}{K_f}} \cdot \gamma \quad \text{..... (5)}$$

ε_{kk} – strain, d'less
t – time, sec
V_o – initial volume, m^3
V – volume, m^3.

Sink rate in the above equations is specified as the volume of the fluid injected per second per unit volume of cement. Using equations (4) and (5), Appleby and Wilson were able to relate the rate of fluid drawn into cement body to cement permeability on one hand and to relate sink rate to cement shrinkage, both bulk and internal, on the other hand. They used Sutton's technique with U-tube measurement to compare their results with Sutton's. The results are

shown in Fig. 6. The data up to 300 min are from Sutton, et al. (1990), while the remaining data are from Appleby & Wilson (1996). The agreement between both methods is good.

These results show that the flow of water through early-time cements may be approximated by Darcy's law, while for late-time cements the model of poroelastic material should be used. Interestingly, the logarithm of cement permeability vs. time yields a straight line. Appleby and Wilson concluded that effective sink rates follow a pattern similar to the level of chemical activity in cement. But perhaps the most important conclusion that can be drawn from these permeability experiments is that cement slurry in its transition phase has enough permeability to enable flow of fluids through itself.

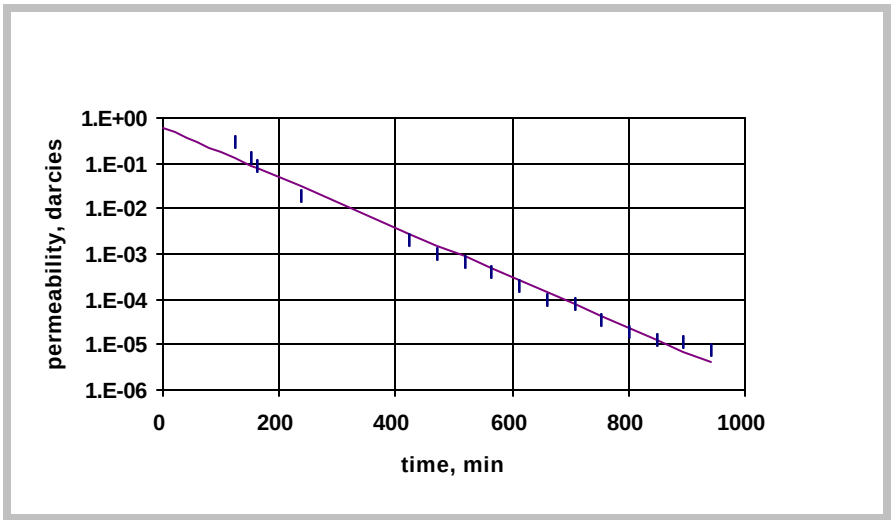

Figure 6. Permeability of fresh neat cement vs. time, after Sutton, et al. (1990) and Appleby and Wilson (1996).

3. MODELING HYDROSTATIC PRESSURE LOSS IN CEMENT COLUMN

3.1 Published Models

The first model of downhole pressure was formulated in the work of Sabins et al. (1980) and takes into account the development of Static Gel Strength (SGS). The pressure differential needed to break gelled cement (Bourgoyne, et al., 1991) is given as:

$$\Delta P = \frac{SGS(z,t)}{300 \cdot (D_h - D_c)} \cdot z \quad \text{..... (6)}$$

where:

SGS – time and depth dependent slurry Static Gel Strength in lbf / 100sq. ft,

D_h – hole diameter, inches,

D_c – casing outside diameter, inches,

z - depth in ft.

Equation (6) is well known in drilling engineering and represents the pressure differential that must be applied to start circulation in a gelled mud-filled annulus. Sabins, et al., postulate that due to some volumetric reduction occurring in the cement column, the column would "like" to

move downward. However, the cement structure represented here by the gel strength opposes any deformation of plastic cement. Cement sticks to the casing and borehole walls, partially supporting itself. As a result, hydrostatic pressure exerted by the cement column is:

$$P_z(z,t) = P_{zi} - P_{SGS} \quad \text{..... (7)}$$

where:

$P_z(z,t)$ – cement column hydrostatic pressure as a function of depth and time,

P_{zi} – cement column initial hydrostatic pressure,

P_{SGS} – pressure loss due to development of SGS, given by eq. 8A.

The point is stressed that the model will lead to a considerable overestimation of pressure loss if deformation due to volumetric reduction is considerably less than the minimum deformation (shear or shear rate) necessary for a given cement slurry to reach SGS.

Work presented by Chenevert and Jin (1989) is an extension of the above model. The basic equation used to model pressure loss is a modified eq. (7). It is given in a differential form to account for time and depth dependent phenomena as:

$$dP = \rho \cdot g \cdot dz - \frac{4 \cdot \tau(\varepsilon)}{D_h - D_c} dz \quad \text{.....(7A)}$$

where:

r – cement slurry density,

g – acceleration of gravity,

t – shear stress at the wall,

D_h, D_c – outer and inner diameter, respectively.

The authors introduced two functions: chemical shrinkage, S(t); and shear stress, $\tau(\varepsilon)$. The former is an empirical relationship obtained in a series of experiments relating volume reduction to time. Density of cement increases as a result of external shrinkage in the following manner:

$$\rho(t) = \frac{\rho_o}{1 - S(t)} \quad \text{..... (8)}$$

where:

ρ_o – initial cement slurry density.

Eq. (8) is derived from a simple consideration of density. If V_S is the volume lost as a result of external (bulk) volume reduction, then:

Chemical shrinkage function S(t) represents a relative volume reduction caused by hydration reactions in cements. A curve of S vs. time presented in the paper shows that neat cements do not lose more than 1% over the first 5-6 hours of their hydration. In such a case density increase is roughly 1% and can be neglected.

The shear stress function is defined as:

$\tau = C \cdot \varepsilon$ *for* $\varepsilon < \varepsilon_c$ ..... (9)

$\tau = \tau_{max}$ *for* $\varepsilon \geq \varepsilon_c$ ..... (10)

where:

ε_c – critical shear strain elastic limit,

C - constant,

τ_{max} – maximum value of shear stress.

The above shear stress function can be visualized in the following graph:

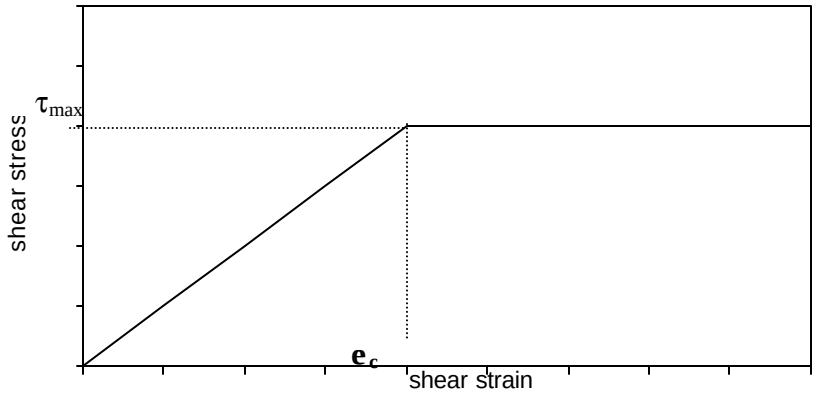

Figure 7. Simple elastic-perfect plastic body, Chenevert & Jin (1989).

This ideal behavior represented by equations (9) and (10) and Fig. 7 does not depart far from reality. In order to characterize cement slurry using the above rheological model, coordinates of only one point are needed (τ_{max}, ε_c). Experimental data for this model were obtained in two steps. In the first step, a dynamic (oscillating) test rheometer was used to determine the elastic shear strain limit. In the second step, a device designed to measure the force required to start movement of a plate immersed in the slurry was used. This served as a means to determine the value of SGS. Chenevert and Jin assumed that the elastic strain limit obtained in oscillatory-type experiments could be correlated with the shear strain corresponding to the static value of the yield point. The researchers did not obtain data for this model using vane geometry, as in the case of Fig. 7. Thus, the assumption discussed above could not be tested. For the sake of comparison, Chenevert and Jin reported that for neat cement @ 30 min. ε_c was 0.1 and τ_{max} was 230 lbf/100 sq. ft.

Haimoni and Hannant (1988) published SGS measurements for cement using vane geometry. They report the value of strain to be 0.003 and shear stress 309 lbf/100 sq. ft @ 15 min. Cement filtration was taken into account using equation (4). The model works as follows:

1. For each time step, total displacement is obtained from filtration and bulk volume shrinkage for each depth z.
2. Using wellbore geometry, displacements are converted into shear strain.
3. Using the relationship $\tau=f(\varepsilon)$, shear stress for each shear strain is obtained.
4. Pressure at each depth and time is computed by means of equation (7).

Haimoni and Hannant report a good correlation of their model with existing data. Although the model is simplistic in many ways (e.g., the stress vs. strain relationship and uniform filtration), it produced good results. The model showed that prediction of downhole pressure is possible.

The model proposed by Daccord et al. (1991) does not introduce any additional physical phenomena. SGS development was modeled using the following exponential relationship:

$$SGS(t) = SGS_o \cdot e^{\frac{t}{t_{rtd}}} \quad \text{..... (11)}$$

where:

SGS_o – initial SGS value,

t - time,

t_{rtd} – characteristic retardation time constant.

Equation (11) is empirical; the initial SGS value represents the first measured SGS. Time constant T_r is found from SGS measurements for a particular cement system. SGS values used in eq. (11) were measured using vane geometry. This method shows superior accuracy for low shear-rate measurements compared with Dzuy and Boger (1983), Haimoni and Hannant (1988), and Meeten and Sherwood (1992). Shrinkage was modeled using the following equation:

$$\frac{dS}{dt} = \frac{S_\infty}{\xi \cdot \sqrt{\pi}} \cdot \exp\left[-\left[\frac{(t-\chi)}{\xi} \right]^2 \right] \quad \text{..... (12)}$$

where:

S_∞ – total shrinkage,

χ, ξ – parameters,

t – time.

Fluid loss was found from Darcy's law in the presence of both mud cake and cement cake:

$$V_{fl} = \frac{1}{\mu} \cdot \frac{\Delta P(z,t)}{\frac{e_c(z,t)}{k_c} + \frac{e_m}{k_m}} \quad \text{.....(1A)}$$

Density change due to volumetric loss is given as:

$$\rho = \frac{\rho_o}{1 - S(t)} + c \cdot P(z,t) \quad \text{..... (13)}$$

where:

ρ_o – initial cement density,

c – cement compressibility,

P – time and depth dependent pressure.

The first term in eq. (13) is identical with that of eq. (8). The second term comes from the density change due to cement compressibility. It should not, however, be linear but exponential.

Two conservation equations are used. The first is an equation of continuity:

$$\frac{\partial \rho}{\partial t} = \frac{\partial (\rho v)}{\partial z} + \frac{4 \cdot \rho_{fl} \cdot D_h}{D_h^2 - D_c^2} \cdot v_{fl}(z,t) \quad \text{..... (14)}$$

where:

ρ – cement density,

ρ_{fl} – fitrate density,

v – cement column velocity,

z – depth,

t – time,

D_h, D_c – wellbore and casing diameter, respectively,

v_{fl} – filtrate velocity.

The first term in eq. (14) represents the rate of mass flow per unit volume, the second represents the divergence of the density-velocity product, i.e., the rate of change of mass per unit volume. The third term is a source/sink term; in this case it represents fluid loss into the wellbore.
The second equation is a balance of forces acting on cement element:

$$\frac{dP(z,t)}{dz} = \rho(z,t) \cdot g - \frac{4 \cdot SGS(z,t)}{D_h - D_c} \quad \text{.....(7B)}$$

where:

g – acceleration of gravity.

Cement moves in this model as a plug, too. Unlike Chenevert and Jin's model, there is only a single SGS value in this model regardless of strain. Some observations the authors made are:

- Top cement displacement due to fluid loss for retarded cements (latex cement) may be as high as 30 ft, and
- Pressure transmission due to slurry permeability may be an important mechanism, especially in shallow wells; characteristic propagation time for a pressure wave in cement was determined to be equal to 23 min for a 300 ft column of cement.

Prohaska et al. (1993) further improved the work of Daccord et al. (1991). The major contribution of this research was that influence of shearing, temperature and pressure on development of SGS was measured using vane geometry. The effect of shear rate was estimated by measurement of SGS after shearing cement samples at different shear rates. It was found out that higher shear rates result in the retardation of the SGS. As temperature increased, development of SGS was accelerated. A similar effect of pressure on SGS development was found. The results derived from this study imply that SGS will develop faster in the lower part of a uniform cement column.

Prohaska et al. (1995) published another model, which is a major refinement of their earlier work from 1993. They introduced the concept of critical distance, which is the distance from the top of the gas zone to the level of pressure balance. Gas pressure is attenuated with depth due to gel strength in the same way that cement pressure is. Within the volume limited by the critical distance, gas pressurizes the whole slurry. Any cement volume reduction within this volume will, therefore, be replaced by migrating gas. Cement shrinkage and filtration are the only sources of

volume loss within the critical distance. According to the researchers, SGS is the source of attenuation of gas pressure propagation within cement column. Nevertheless, Prohaska claims that gas intake into the column of cement occurs in the form of small bubbles that coalesce into a large one. Once a single bubble reaches a critical bubble size it can detach from the walls and migrate upward. SGS is the only opposing force preventing the detached gas bubble from moving upward. The researchers noticed during their experiments that, when SGS reached the value of 600 lbf/100 sq. ft, the only mechanism for migration was a piston-like displacement of cement by gas. The value of 600 lbf/100 sq. ft appears, however, to be related to the particular geometry of pipes used in the experiments. This observation implies that a very high gas pressure would be necessary for gas to flow in a slurry that has SGS value over this critical value because gas would have to overcome not only the resistance coming from the SGS, but also would have to lift the whole slurry (piston-like displacement). For example for a 14.75”/10.75” annulus and cement density 16.4 ppg, and gas migrating from 3000 ft, this pressure would have to be 4058 psi, i.e., the gas zone pore pressure gradient would be 26 ppg.

Contrarily, most gas flow events occur at least two hours after cement has been pumped, i.e., while SGS has a value of around 500 lbf/100 sq. ft. Also, gas test cells confirm that such a high pressure is not necessary. Substantial evidence from field data, as well gas cell tests, indicate that gas does not have to migrate in cement slurries by slug flow. A degenerated, highly porous cement matrix was observed in gas migration test cells. Also, once a gas bubble detaches, no further pressure support from the bottom exists, and the only driving force for its upward movement is buoyancy. It has been established in the area of two-phase flow, however, that a yield point of 25 Pa (50 lbf/100 sq. ft) is enough to prevent bubbly flow of gas in liquids (Beris, et al., 1985).

Sabins and Wiggins published results of their modeling in 1994. They assumed that the initial set is the ultimate criterion for cement to resist gas migration. They observed that at this point SGS reaches the value of 2000 lbf/100 sq. ft. Three aspects of flow after cementing were addressed: physical properties of cement slurry; pressure loss in a column of setting cement; and the influx of gas into the column of cement. The physical phenomena leading to the pressure loss are the same as in previous models: the combination of volumetric reduction and SGS development. SGS as a function of time was found using a Max Analyzer (a customized cement consistometer). Volumetric loss in hydrating cement and permeability of the hydrating cement were modeled as functions of SGS. Fluid loss was estimated using the following empirical relationship:

$$V_{fl} = 2 \cdot A \cdot C_c \cdot \left[\sqrt{\frac{C_c^2}{C_{df}^2} \cdot t_{df} + t_c} - \sqrt{\frac{C_c^2}{C_{df}^2} \cdot t_{df}} \right] \quad \text{..... (15)}$$

where:

A – area of fluid loss,

C_{df}, C_c – fluid loss coefficients for the drilling fluid and cement slurry, respectively,

t_{df} – time of fluid loss for drilling fluid,

t_c – time of fluid loss for cement.

In order to obtain a pressure drop, two equations are used: Darcy equation and eq. (6). Sabins and Wiggins postulate that cement slurry in its transitional phase behaves like a porous

body and that the Darcy equation describing flow of water through the permeable cement matrix is valid. Flow of interstitial water compensates for the volume reduction due to hydration and filtration. The assumption is made that there is an infinite source of water on the top of the cement column. The researchers also claim that SGS limits the pressure drop for the flow of interstitial water in the cement matrix in such a way that, if volume losses produce a potential pressure loss less than that allowed by the SGS, the actual pressure drop is computed using the Darcy equation. On the other hand, if a volume change occurs that would produce a larger pressure loss than that permitted by SGS development, a downward movement of the column will occur.

In this model, the assumption is also made that the top portion of the cement column requires a rate of water through the cement permeability that is equal to all the volume losses in the well below that point. This assumption is not valid because of the effect of compressibility of water in pores. Moreover, a mutual dependence exists between the pressure loss due to the SGS development and the flow of interstitial water. That is, any amount of water flowing into a given volume of cement will decrease strain in that volume; therefore, it will decrease pressure loss due to SGS, which, according to the researchers' hypothesis, will in turn influence the rate of water influx into that volume. The flow of interstitial water through the cement matrix is a time-related phenomenon. As mentioned before, the characteristic time of pressure wave propagation was estimated to be 23 minutes for a 300-ft cement column. Apparently, this time was not taken into account in the model. Additionally, in the model assumes that the volume of gas entering into the cement column is approximated by the volume of fluid lost in the cement column across from it. The authors concluded from the model that fluid loss, SGS, and overbalance pressure affect gas migration the most. Cement permeability, on the other hand, was found not to affect the problem significantly. To improve the model, cement permeability could be related to filtrate volume, as water deficiency may result in cement dehydration and in effect, pores may not be plugged with hydration products.

In summary, the pressure loss models described herein represent a high level of sophistication and a significant theoretical contribution to our understanding of the mechanisms occurring in the hydrating cement that lead to the loss of pressure and flow of formation fluids. None of the more advanced models, however, can be practically used because all of them require a large amount of input data, such as detailed properties of the cement and location and properties of gas or water zones in the open section of the wellbore. Routinely, no such data is available in a complete form. Moreover, the quality of most of the available data is often poor. Consequently, pressure prediction models remain as analytical tools that help qualify the relative importance of specific mechanisms.

3.2 Cement Pressure-Unloading Model

Pressure unloading model, developed in this project, considers pressure transient effect resulting from propagation of volumetric reduction caused by bottomhole fluid loss (Nishikawa, 1999). The process is described as follows.

After the cementing job is completed, the column of cement slurry in the open hole annulus starts losing water to the rock because of pressure overbalance and filtration. Expansion of volume through fluid loss causes pressure reduction due system compressibility. Also, as the fluid loss continues, part of the cement slurry moves downward in the plug flow fashion. This downward movement of the cement slurry generates friction at the annular walls, which reduces the hydrostatic pressure. A pressure unloading (transient) effect is generated and transmitted

upward from the point of the fluid-loss zone to the surface. As a result, pressure reduction along the cement column becomes a function of time and depth. To derive a mathematical model, the following assumptions have been made:

- There is only one fluid-loss zone and one gas zone in an open hole, and the fluid-loss zone is located near the gas zone (Fig. 8).
- Only the fluid loss contributes to volumetric change. At early time, chemical shrinkage is small and does not cause a hydrostatic pressure loss.
- The hydrostatic pressure loss continues until it balances the pressure of the fluid-loss zone (Cooke, et. al, 1983).
- The fluid loss is mostly controlled by a pressure differential (Haberman, et. al, 1992), and the permeability of a mud cake at the wall is approximately constant (Abboud, et. al, 1997).
- Cement slurry density and compressibility are constant.
- A plug flow model describes a motion of the cement slurry.
- Cement slurry rheology is constant during the early time after cement placement; the gel strength value is constant during the dormant period of slurry setting.
- The pressure of the gas zone is higher than that of the fluid-loss zone (Fig. 8).
- The pressure gradient of the gas zone is higher than that of the fluid-loss zone.

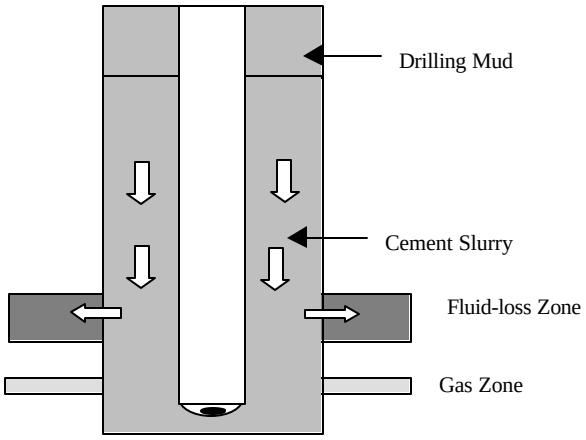

Figure 8. Cement pressure - unloading model.

The flow equation is

$$\frac{\partial p}{\partial t} = c^2 \frac{\partial^2 p}{\partial x^2}, \qquad (16)$$

where:

$$c = \sqrt{\frac{c_1}{c_2 V}} \qquad (16A)$$

$$c_1 = \frac{60000(r_2 - r_1)^2}{m_p}\left[1 + \frac{3}{2}\frac{\tau_y}{\tau_{SGS}} - \frac{1}{2}\left(\frac{\tau_y}{\tau_{SGS}}\right)^3\right] \qquad (16B)$$

c_2 = compressibility of the cemented annulus (1/psi)

τ_y = yield point (dyne/cm^2),

τ_{SGS} = static gel strength (dyne/cm^2),
μ_p = plastic viscosity (dyne-s/cm^2),
V = fluid volume in the annulus (cm^3), and
x = depth (cm).

After solving the equation of flow, we derived the *pressure unloading model* formula as:

$$p(x,t) = 0.052\rho_f x + 2\sum_{n=1}^{\infty} \frac{0.052}{L}\left(\rho_c - \rho_f\right)\left(\frac{(-1)^{n+1}}{a^2}\right)\sin[ax]\cdot e^{-c^2a^2t} \qquad (17)$$

where:
ρ_f = equivalent density of normal formation pressure gradient (ppg),
ρ_c = density of the cement slurry (ppg),
L = bottom of cement (cm), and
α = constant defined as:

$$\alpha = \left(n\pi - \frac{\pi}{2}\right)\frac{1}{L} \qquad (17A)$$

The results of calculations using Eq. (17) can be verified using material balance calculations. The hydrostatic pressure loss produces a volume increase in an annulus because of the annular system compressibility, c_2. The volume increase represents water lost to the formation. Thus, the fluid loss is given by:

$$V_f = c_2 V \overline{\Delta p} \qquad (18)$$

where:
V_f = fluid loss (ft^3),
V = volume of the cement slurry (ft^3), and
$\overline{\Delta p}$ = average pressure drop in the annulus (psi).

The new model does not consider the effect of SGS development on a hydrostatic pressure loss. Using the results from Manowski (1997), we assumed that at early time the SGS effect is much smaller that that of the fluid loss. At later time, the SGS effect becomes large and should affect the hydrostatic pressure loss. Approximately two hours after cement placement, SGS development should not be ignored.

To qualify the effect of the yield point–SGS ratio, we used Eq. (17) by the proper ratio between 0.30 and 0.50 (Hanks, et. al, 1967). The geometry used in these calculations is shown in Table 3. As shown in Fig. 9, the three ratios display no significant differences.

Table 3. Input Data for Comparison of Yield Point and SGS

Outside diameter	(in)	19
Casing OD	(in)	13.375
Total compressibility (10^-6)	(psi^-1)	20
Cement slurry density	(ppg)	15
Cement column length	(ft)	4,000
Depth of interest	(ft)	4,000
PV	(cp)	200
YP/SGS		0.3-0.5
Formation pressure gradient	(ppg)	8.9

This result reveals that SGS development is not sensitive to the hydrostatic pressure loss in the model as long as the proper range of 0.30 <YP/SGS<0.50. The SGS is almost constant in early time after placement. However, as shown in field experimentation (Cooke, et. al, 1983), the hydrostatic pressure loss was dramatically changed until 120 minutes after cementing. From the data resulting from the field experiment and the above calculation, we concluded that the SGS development is not largely influenced in early time after placement when most of the hydrostatic pressure loss occurs.

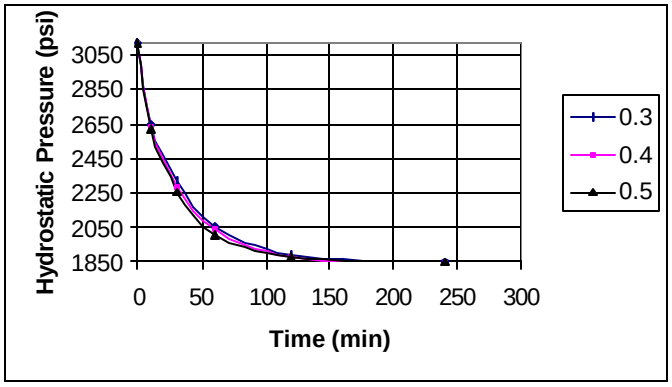

Figure 9. Hydrostatic pressure loss for various YP/SGS ratios

3.2.1 Pressure Unloading Model Verification with Field Data

The hydrostatic pressure data from the field experiment are given Table 4 (Cooke, et. al, 1983).

Table 4. Field Test Data

Time (min)	@ 8,754 ft (psi)	@ 6,909 ft (psi)	@ 5,488 ft (psi)	@ 4,787 ft (psi)	@ 4,632 ft (psi)	@ 3,636 ft (psi)
0	7,100	5,450	4,200	3,550	3,400	2,600
50	5,850	4,600	3,750	3,250	3,100	2,300
150	5,000	3,900	3,200	2,600	2,500	2,100
340	4,150	3,150	2,550	2,300	2,050	1,700
400	4,150	3,150	2,550	2,300	2,050	1,700

Manowski (1997) conducted an experiment to measure compressibility of a neat slurry by simulating the borehole effect. The compressibility was almost constant over 2,000 psi of applied pressure. This constant number was used in the calculations below. Input data for the calculations are shown in Table 5.

Table 5. Input Data

Outside Diameter*	(in)	9.0
Casing OD	(in)	2.875
PV	(cp)	200
YP/Shear Stress		0.4
Total Compressibility	(psi-1)	20×10^{-6}
Formation Pressure Gradient	(psi/ft)	0.465
CMT Weight	(ppg)	15.65
CMT column Length	(ft)	8900

* 10% washout of 7 7/8" hole

Results of hydrostatic pressure change are shown in Table 6 and in Figs. 10 and 11.The results show that this model gives a very good match with the data of the field experiment.

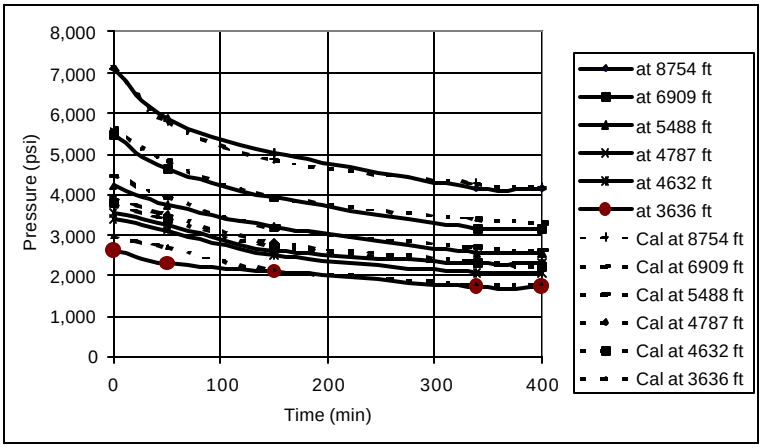

Figure 10. Validation of cement pressure-unloading model

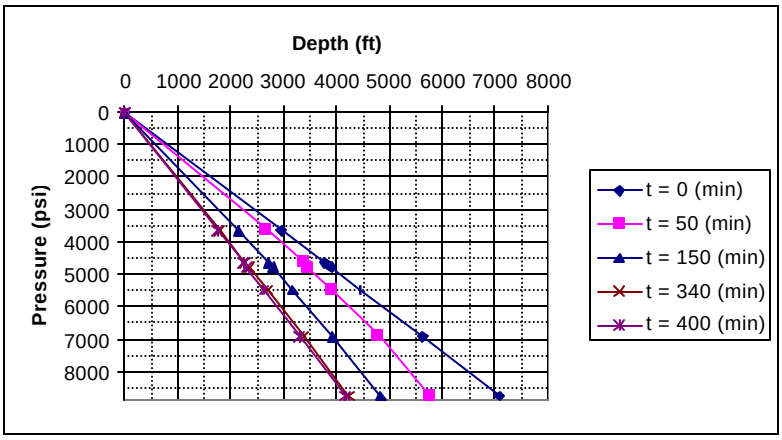

Figure 11. Hydrostatic pressure in cement at various times

Table 6. Hydrostatic Pressure Distribution in Cement vs. Time

Time (min)	@ 8,754 ft (psi)	@ 6,909 ft (psi)	@ 5,488 ft (psi)	@ 4,787 ft (psi)	@ 4,632 ft (psi)	@ 3,636 ft (psi)
0	7,105	5,626	4,462	3,900	3,773	2,958
50	5,783	4,817	3,954	3,496	3,392	2,703
150	4,853	3,947	3,196	2,811	2,724	2,159
340	4,248	3,380	2,698	2,359	2,283	1,797
400	4,182	3,318	2,644	2,310	2,235	1,757

In Table 7, errors between the calculations and the field data are shown. The values do not exceed 10% error. Thus, the model seems adequate to calculate the hydrostatic pressure after cement placement.

Table 7. Percent Error between Experiment and Calculations

Time (min)	8,754 (ft)	6,909 (ft)	5,488 (ft)	4,787 (ft)	4,632 (ft)	3,636 (ft)
0	0.07%	3.13%	5.87%	8.97%	9.89%	12.10%
50	1.16%	4.50%	5.16%	7.04%	8.61%	14.91%
150	3.03%	1.19%	0.13%	7.51%	8.22%	2.73%
340	2.31%	6.80%	5.49%	2.50%	10.21%	5.40%
400	0.77%	5.06%	3.56%	0.43%	8.28%	3.24%

The model is also verified by comparing the effects of fluid loss (top cement movement) and pressure unloading (compressibility). The fluid loss is calculated from Eq. (18) using average hydrostatic pressure reduction, p, as:

$$V_f\ (cu.ft.) = c_2 V \overline{\Delta p} = 20\times10^{-6}\times\frac{(9^2 - 2.875^2)}{1{,}029.4}\times 5.615\times 8{,}900\times\frac{\text{Measured Pressure @ } 8{,}900\,\text{ft}}{2}$$

Note that average pressure in the well is calculated from the recorded pressure @ 8,900 ft. shown in Fig. 12. Also, the calculated volume of fluid loss and vertical drop of the top cement corresponding to that volume are plotted in Fig. 13. The calculated 270-ft cement level drop corresponds very well to the drop of 300 ft measured in the field experiment by Cooke, et. al (1983). Thus, we conclude that the pressure loss at the cement bottom results from volumetric expansion (fluid loss) and compressibility of the system (pressure unloading).

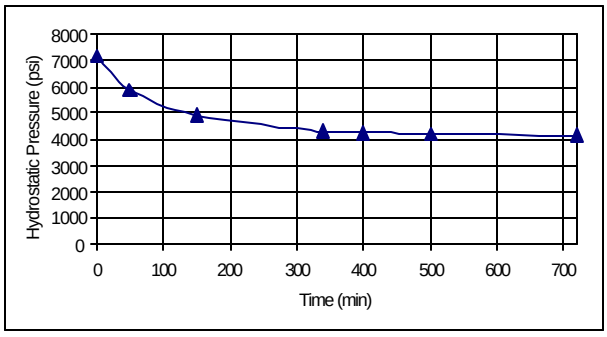

Figure 12. Measured hydrostatic pressure reduction at 8,900 ft

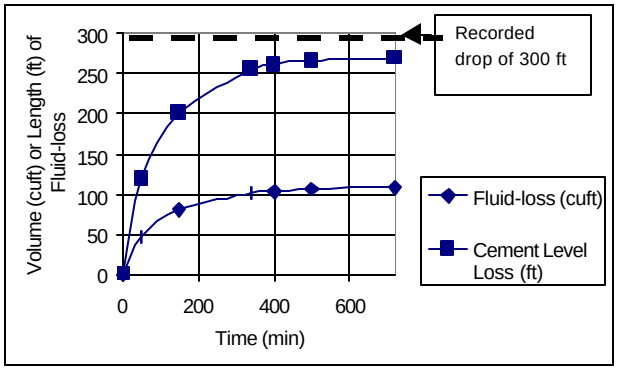

Figure 13. Fluid loss and cement top drop

3.2.2 Sensitivity of Pressure Unloading Model

We conducted a sensitivity study of the pressure unloading model, Eq. [17], to evaluate the effects of annular geometry and compressibility on hydrostatic pressure loss in the cement column. Geometry of an example well considered in the study is shown in Fig. 14. A 13 3/8-in. casing is run to a depth of 4,000 ft, where a fluid loss zone is assumed to occur. The gas zone, which has a pressure larger than that of the fluid loss zone, is located just below the fluid loss zone. To simplify conditions, there is no mud column on top of the cement. The study also includes the effect of fluid loss.

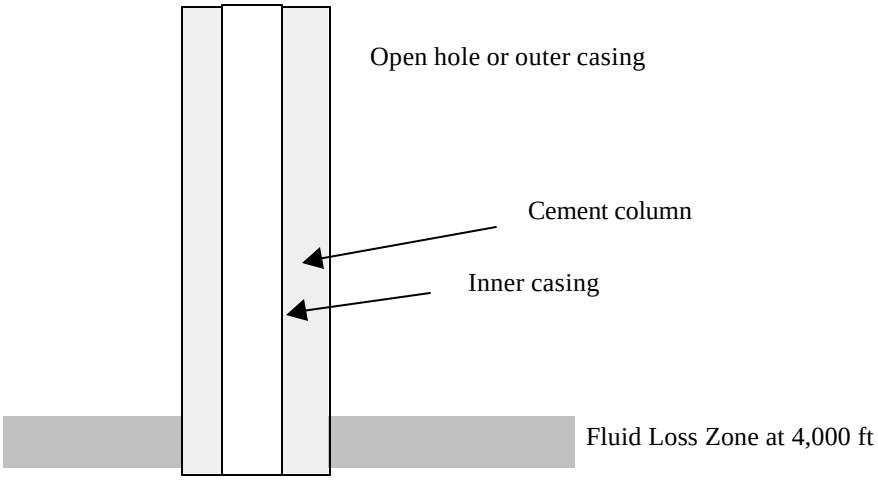

Figure 14. Configuration of an example well for sensitivity study.

Effect of Annular Size

First, the effect of the annular dimension was calculated using hole sizes between 16 in. and 20 in. (Table 8). The results are shown in Fig. 15 and indicate that a large annulus would accelerate the process of pressure loss after cement placement. It would also require large fluid loss - as shown in Fig. 16. *Thus, a large annulus with high water loss would give quick and large reduction of hydrostatic pressure in the cement column and more likely intrusion of gas.*

Table 8. Input Data: Effect of Annular Size

Outside diameter	(in)	18-20
Casing OD	(in)	13.375
Total compressibility (10^-6)	(psi^-1)	20
Cement density	(ppg)	15
Cement column length	(ft)	4,000
Depth of interest	(ft)	4,000
PV	(cp)	200
YP/SGS		0.4
Formation pressure gradient	(ppg)	8.9

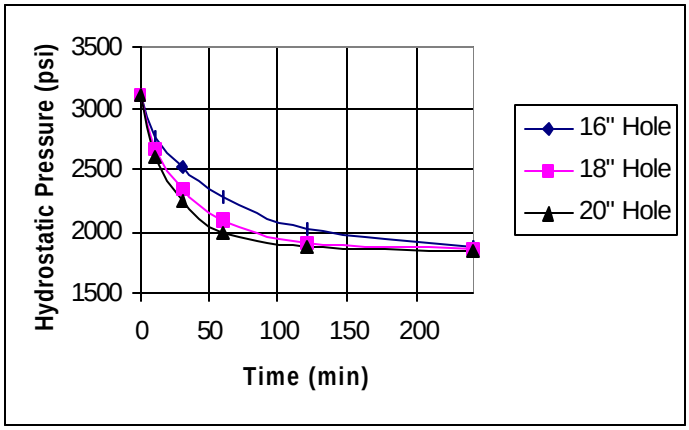

Figure 15. Effect of annular size on pressure loss in cemented annulus

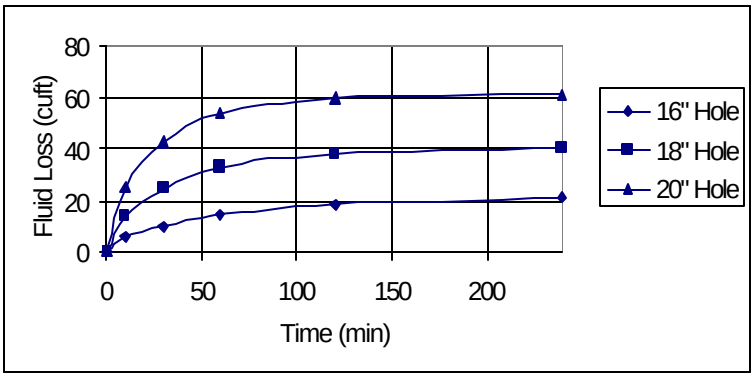

Figure 16. Effect of annular size on cement slurry fluid loss

Compressibility Effect

The effect of compressibility was studied using the compressibility values between 10×10^{-6} and 20×10^{-6} (Table 9). The results in Fig. 17 indicate that pressure loss in cement occurs earlier and faster in cements with small compressibility of the annulus. Also, comparison of the plots in Fig. 17, and Fig 18 indicate that for a low-compressibility system the fluid loss of 20 cu. would result in 1,100 psi pressure drop, as compared to 500 psi for high-compressibility system. *Thus, the annular cement system having large compressibility would be more tolerant to fluid loss in terms of losing hydrostatics than the low-compressibility system.*

Results from the sensitivity study can be summarized as follows:

- Large annuli accelerate and pronounce hydrostatic pressure loss; and
- High compressibility reduces hydrostatic pressure loss.

The first observation implies that surface holes should be more sensitive to gas migration than deep holes. Also, cement slurry filtration should be minimized in surface holes. The second observation emphasizes the importance of determining the annular system compressibility that

includes the open-hole lithology. Further investigations are required for a proper evaluation of compressibility.

Table 9. Input Data: Effect of Compressibility

Outside diameter	(in)	19
Casing OD	(in)	13.375
Total compressibility (10^-6)	(psi^-1)	10-20
Slurry density	(ppg)	15
Cement column length	(ft)	4,000
Depth of interest	(ft)	4,000
PV	(cp)	200
YP/SGS		0.4
Formation pressure gradient	(ppg)	8.9

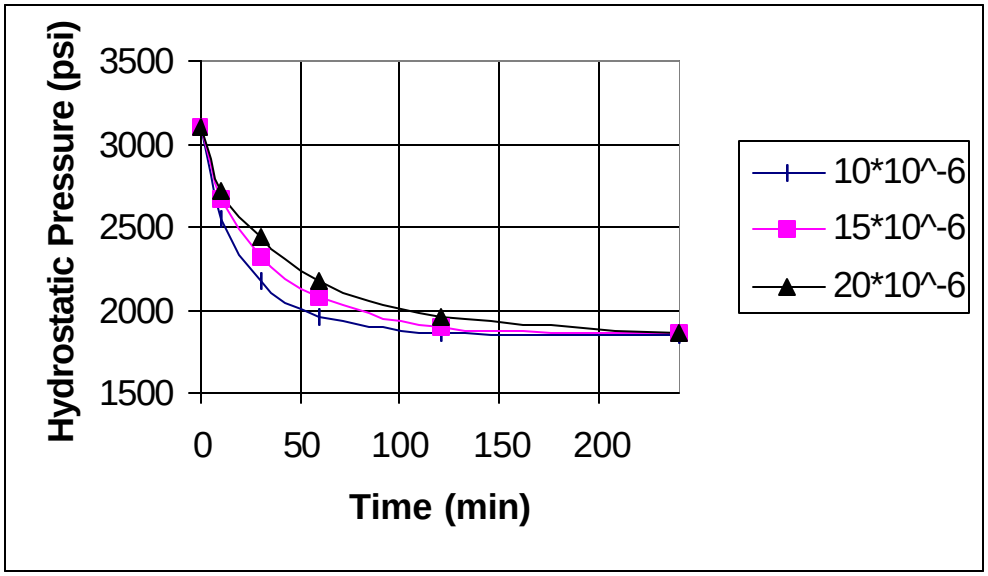

Figure 17. Effect of compressibility on pressure loss in annular cement

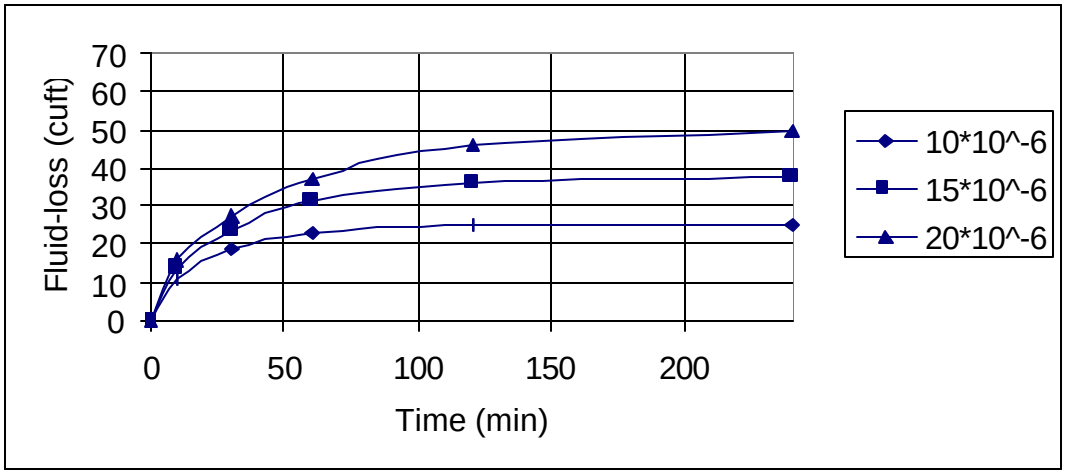

Figure 18. Fluid loss for various annular compressibilities.

4. FIELD PRACTICES AND PROCEDURES FOR PREVENTING FLOW AFTER CEMENTING

Realizing that it was much more difficult and costly to control an existing flow and eliminate all its consequences than to prevent it, operators have developed practices to minimize the chance of flow after cementing in areas where flow after cementing occurs frequently. In principle, these practices are based on a careful cementing job design and its proper execution. Presented here are results of a survey involving industry data, expert interviews, and technical literature regarding these methods. This summary includes technical requirements and procedures for preventing early gas migration after cement placement.

4.1 Technical Requirements

The design and execution of a cementing job in an area with potential gas migration is different for shallow and deep water applications. Summarized in Table 10 below is a sequence of operations leading to successful cementing operations in shallow and deep water wells.

Table 10. Technical Requirements for Anti-gas Cementing

Operation/Property:	**Shallow Water Cementing:**	**Deep Water Cementing:**
Mud Design	flat gel strength, low fluid loss, firm, thin filter cake	same as shallow water
Mud Conditioning	to eliminate gels and erode excessive filter cakes, Hartog et al. (1983)	not applicable
Viscous Pills (Sweeping Fluid)	not applicable	remove cuttings from the borehole and provide adequate filter cake, foamed fluids becoming very successful due to their versatility and high density flexibility
Spacer	pumped to separate mud from cement and to wet surface of rock and casing in case of oil base muds, Hartog et al. (1983)	not applicable
Spotting Fluid (Kill Mud)	not applicable	stabilizes the wellbore, recently settable fluids have been designed to provide a settable filter cake, activated by cement slurry
Mud Displacement	turbulent flow regime if possible, minimum contact time 4 min., Marlow (1989)	usually plug flow
Casing Centralization,	all achievable	centralization difficult to achieve,

Reciprocation and Rotation		casing cannot be moved
Fluid Density Hierarchy	fluid pumped denser by 10% than fluid displaced	difficult to achieve due to narrow margin between pore pressure and frac gradient
Fluid Frictional Losses Hierarchy	fluid pumped having 20% more frictional losses than fluid displaced	achievable
Cement Free Water and Sedimentation	zero, Webster & Eikers (1979)	Zero
Cement Filtration	less than 50 ml in API HTHP test, 1000 psi differential pressure, Cook & Cunningham (1976) Garcia & Clark (1976)	less than 50 ml in API HTHP test, 1000 psi differential pressure,
Thickening Time	cement should start to set from the bottom up immediately after placement, Marlow (1989)	same as shallow water
Transition Time	minimum	minimum
Rheology	optimized so that frictional pressure losses follow the above hierarchy, ECD must not exceed fracturing gradient of the formation	difficult to achieve due to narrow margin between pore pressure and fracturing gradient
Compressive Strength	must be in the order of 500 psi in 24 hr at bottom hole conditions	difficult to achieve at low temperature and for low density cements typically used, must use special cements

4.2 Operator's Procedures for Prevention of Flow after Cementing

Current procedures for preventing flow after cementing involve the following steps:

1. Identifying areas with flow problems;
2. Determining accurate pore pressures, fracturing gradients, as well as lithology, often using MWD and LWD;
3. Carefully designing mud/spacer/cement systems according to the technical requirements outlined above with special emphasis on filtration control;
4. Applying special cements designed specifically to perform in wells with gas flow potential;
5. Using automated cementing equipment for quality control. The benefits from using the equipment include:

- eliminating human error;
- obtaining uniform properties of cement slurry;
- mixing additives accurately.

6. Accurately adding and uniformly distributing cement additives. Inaccurate additions and non-uniform distribution of additives has been identified as one of the primary reasons for poor quality cementing jobs.

The survey presented above leads to the following conclusions:

- Operating companies avoid using special cements on a routine basis due to cost; they stress good fluid design, mud displacement and supervision.
- If a well is drilled in an area known to have given severe problems in the past, special cements are used regularly.
- Only one operating company uses laboratory tests of gas migration in order to screen various cement compositions for the cementing job.

Appendix B summarizes present techniques and procedures used by some operators in the Gulf of Mexico.

5. PREDICTION OF POST-CEMENTING FLOW HAZARD

The purpose of this research was to find a simple screening method for calculating the risk of flow after cementing. On one hand the method must consider properties of cement slurry together with geological conditions, while on the other hand it must give a simple quantitative criterion for comparison between high-risk and low-risk cementing operations. In addition, the method's reliability must be verified using data from actual wells with and without flow problems in order to show that the calculated risk correlates with the real one.

5.1 Risk Indicators of Flow after Cementing

Flow Potential Factor

The flow potential factor was developed as a predictive tool in 1984. The concept is based on the pressure reduction caused by the development of static gel strength (SGS) in the presence of cement volume reduction. The critical condition for gas entrance is the equality of gas formation pressure and cement column hydrostatic pressure:

$$P_h(h,t) = P_{gas} = P_{hi} - P_{SGS} \quad \text{..... (19)}$$

where:

P_{gas} – gas zone pore pressure,

P_{hi} – initial hydrostatic pressure of the cement column,

P_{SGS} – pressure loss due to the SGS development.

The critical condition for equality of pressures can expressed as:

$$\frac{P_{SGS}}{P_{hi} - P_{gas}} = 1 \quad \text{..... (20)}$$

A number of laboratory experiments that include injecting gas into a column of setting cement have been performed in order to obtain a minimum SGS value at which gas will not flow through cement. The experiments were conducted in a 3/80 by 20 12.5-ft long annulus. A detailed description of the experimental procedure can be found in Tinsley et al. (1979). The experiments have shown that cement that develops the static gel strength value of 500 lb. per 100 sq. ft is virtually impermeable to gas percolation. The pressure loss equivalent to this SGS value is called the maximum pressure reduction (MPR). In field units this equation is:

$$P_{SGS} = SGS \cdot \frac{z}{300 \cdot (D_h - D_c)} \quad \text{.....(8A)}$$

and Maximum Pressure Reduction is:

$$MPR = \frac{500}{300} \cdot \frac{z}{(D_h - D_c)} = 1.67 \cdot \frac{z}{(D_h - D_c)} \quad \text{..... (21)}$$

The flow potential factor (FPF) is defined as the ratio of the MPR to the initial overbalance pressure (OBP):

$$FPF = \frac{MPR}{OBP} \quad \text{..... (22)}$$

where the initial overbalance pressure is defined as the initial cement column hydrostatic pressure minus the gas zone pressure. The nitrogen gas used in the experiments was injected in slugs of 100 cubic centimeters, rather than continuously. In such a case, there is no continuous pressure support of the migrating gas from the bottom. It was established in the past that in the case of bubble flow, gel strength of ca. 50 lb./100 sq. ft is enough to stop a bubbly flow of gas (Beris et al., 1985). The value of 500 lb./100 sq. ft obtained in the experiments is a derivative of the specifics of the given experiment, i.e., the geometry of the pipe used. Simple computations show that a much lower value of surface tension is needed to stop bubbles from migrating upward if the only driving force is buoyancy. Another argument against the FPF concept is that it is based on the premise that gas percolation involves breaking the cement slurry structure, i.e., percolating gas bubbles need to overcome the yield point of the slurry. This hypothesis is questionable (Cheung & Beirute, 1982; Rae & Free, 1989; Stewart and Schouten, 1986; Sabins and Wiggins, 1994).

Gas migration has often been noticed to occur as flow through a porous, degenerated cement rather than through a single continuous channel. It is doubtful whether SGS is the force that must be overcome for such a mode of migration to happen. Moreover, for a typical non-retarded slurry, SGS reaches the critical value of 500 lb./100 sq. ft no later than 3 hours after pumping is over. Most occurrences of gas flow were reported to happen well after 3 hours, i.e., when SGS should reach a value well over 500 lb./100 sq. ft.

Slurry Response Number

The concept of the slurry response number (SRN) relies on the observation that cements that exhibit low fluid loss and short transition time generally tend to exhibit good gas migration control (Bour and Wilkinson, 1989; Sutton and Sabins, 1990; Harris et al., 1990). The SRN can be expressed in terms of rate of increase of SGS and fluid loss (Sutton and Ravi, 1989):

$$N_{SG} = \frac{\frac{d(SGS)}{dt}}{(SGS)_x} \quad \text{..... (23)}$$

$$N_{FL} = \frac{\frac{dv_{fl}}{dt}}{\frac{V}{A}} \quad \text{..... (24)}$$

$$SRN = \frac{N_{SG}}{N_{FL}} \quad \text{..... (25)}$$

where:

N_{SG} – static gel strength number, s^{-1}

N_{FL} – fluid loss number, s^{-1}

$\frac{dv_{fl}}{dt}$ = filtrate penetration rate, in / min

SRN – Slurry Response Number, dimensionless

$(SGS)_x$ – SGS at which maximum increase of SGS occurs, lbf / 100 sq. ft

V - unit annulus volume, in^3

A - unit borehole wall area, in^2.

The filtrate penetration rate is obtained from the API filtration test in such a way that, at each time step, the incremental volume of filtrate needs to be computed. Filtrate penetration rate is the volume of filtrate collected at a time step divided by the time step and by the filtration area. A serious drawback of the SRN indicator is that it does not take into account pressure behavior in the annulus. In fact, the SRN numerical value depends almost exclusively on cement properties, i.e., cement gellation and fluid loss. The borehole volume/area ratio does not change very much in conductor and surface casing cementing. Another disadvantage of SRN is that the number does not represent any physical phenomena. It has only a relative meaning, i.e., a higher value is better than a lower one. SRN has been disqualified for the purpose of this study because it is not a good predictor of gas migration severity. However, SRN could be a good way of screening cements for gas migration problems.

Slurry Performance Number

The slurry performance number (SPN) comprises four different factors that are believed to be important in the evaluation of gas migration severity (Rae et al., 1989):

- formation factor,
- hydrostatic factor,
- mud removal factor, and
- slurry performance factor.

Formation factor (FF) is defined as the ratio of gas formation capacity (the product of formation permeability and formation thickness) to the cement pore space critical volume. The latter is defined as the minimum volume that gas needs to occupy in the annulus before gas can

migrate freely up to the surface. This volume is computed in such a way that an annular volume of cement from the top of the gas zone up to the point of pressure balance, between the gas pressure and the hydrostatic pressure exerted by the cement column, is computed first. Next, cement porosity of 2% is assumed. Based on this assumption, the critical volume is equal to 2% of the computed annular volume. Numerically, FF is defined in the following manner. If P_g is gas formation pressure, then we are looking for such a depth L at which P_g is equal to the initial hydrostatic pressure exerted by the cement column, i.e.:

$$L \cdot \rho_c \cdot 0.052 = P_{gas} \quad \text{..... (26)}$$

where:

ρ_c – cement density in ppg,

L - depth to pressure balance in ft,

P_{gas} – gas formation pressure in psi.

Then if L_{gas} is the depth to the gas zone, critical distance is

$$L_c = L_{gas} - L \quad \text{..... (27)}$$

and critical volume is the critical distance times 2% times annular cross - section, or:

$$V_c = 0.02 \cdot \frac{\pi}{4} \cdot \frac{D_h^2 - D_c^2}{144} \cdot \left(L_{gas} - L \right) = 0.02 \cdot \frac{\pi}{4} \cdot \frac{D_h^2 - D_c^2}{144} \cdot \left(\frac{P_{cg} - P_{gas}}{0.052 \cdot \rho_c} \right)$$

where:

D_h, D_c – borehole and casing diameter respectively, in,

P_{cg} – cement hydrostatic pressure opposite the gas zone,

then Formation Factor is:

$$FF = \frac{kh}{V_c} = \frac{476.7 \cdot kh \cdot \rho_c}{OBP \cdot \left(D_h^2 - D_c^2 \right)} \quad \text{..... (28)}$$

where:

k – gas zone permeability, md,

h – gas zone thickness, ft.

It is important to notice that, in computing the depth of pressure balance, neither the hydrostatic pressure loss in the cement column nor the gas pressure decrease are taken into account. Moreover, it is not quite clear what the physical meaning of the critical distance L_c is. Since below the balance depth, the hydrostatic pressure is greater than the gas zone pressure, gas cannot enter and charge cement within the critical distance. It can, indeed, flow into cement only when the hydrostatic pressure exerted by the cement is less than the gas zone pressure. In this case, however, one cannot compute critical volume according to this procedure. Another point that should be made is that initial overbalance pressure, while important in this procedure, may

not be as critical in real life. The principal property of the cement/wellbore system is how fast and how much the hydrostatic pressure exerted by the cement column drops.

Hydrostatic factor (HF) is a ratio of gas zone pore pressure to initial cement column hydrostatic pressure, i.e.:

$$\mathrm{HF} = \frac{P_g}{P_{cg}} \quad \text{..... (29)}$$

Again, pressure loss in the cement column is not taken into account in this method.

Mud removal factor estimates mud removal from the annulus before cementing. The numerical value of the mud removal factor is estimated on the basis of judgment rather than any computations.

Finally, the s*lurry performance number* (SPN) estimates the fluid loss in the transition stage between the initial and final cement sets. Both the initial and final cement sets are estimated using the API consistometer data. The initial set is defined as time to reach 30 B_c (Bearden units of consistency), while the final cement set is defined as time to reach 100 B_c. Fluid loss data is determined from the API fluid loss test. The SPN is numerically defined as:

$$SPN = \frac{V_{fl} \cdot \left[\left(t_{100Bc} \right)^{0.5} - \left(t_{300Bc} \right)^{0.5} \right]}{\sqrt{30}} \quad \text{..... (30)}$$

where:

V_{fl} – API fluid loss, ml in 30 min.,

t_{100Bc} – time to 100 B_c, in minutes,

t_{30Bc} - time to 30 B_c, in minutes.

Cements exhibiting high filtration and long transition time are assigned as high-risk cements according to the SPN procedure. This method has two serious drawbacks. First, it is not easily applicable due to data requirements. Usually, one does not have good data for gas zone depth and pore pressures, not to mention permeability and thickness. Second, the method completely ignores the pressure loss in the column. Different cements in different geological conditions will lose pressure in different manners, and these differences are not taken into account in this method. The SPN method, due to its data requirements, could not be used in this study.

5.2 Correlation of Risk Indicators with Field Case Histories

In order to analyze past incidents of flow, gas FPFs for the sixteen case histories in Appendix A were computed. Also, data from fourteen wells where flow did not occur have been acquired from the MMS statistics to compare both groups and find if the values of a risk indicator for flowing and non-flowing wells are significantly different. Data from the non-flowing wells is shown in Table 11. Also, the calculations of the FPF are shown in Table 12.

Table 11. Summary of Non-Flowing Wells in GOM

Case #	Date	Rig Type	Conductor Casing		Surface Casing		Cement Weight		Pore Pressure ppg
			Depth ft.	Diameter in.	Depth ft.	Diameter in.	Lead ppg	Tail ppg	
1	5/8/91	Jackup	1000	20.00	5000	13.375	11.4	16.2	9.9

2	11/22/92	Jackup	1200	20.00	4000	13.375	11.5	16.4	9.2
3	4/18/93	Jackup	1000	20.00	4000	13.375	12.7	16.4	9.0
4	10/21/83	Platform	800	16.00	1600	10.75	11.4	16.2	8.8
5	2/25/93	Platform	2150	16.00	3500	10.75	13.1	16.2	9.0
6	3/27/94	Jackup	2150	24.00	3500	10.75	13.1	16.2	9.0
7	1/8/89	Platform	750	16.00	3000	10.75	16.2	16.2	8.8
8	7/19/94	Platform	465	24.00	5492	10.75	16.2	16.2	8.8
9	5/26/83	Platform	465	24.00	3300	10.75	12.0	16.4	9.0
10	2/14/78	Jackup	900	13.375	2150	9.625	12.5	16.4	9.5
11	6/1/79	Jackup	900	20.00	3100	13.375	12.5	16.4	8.8
12	9/16/65	?	900	16.00	3000	10.75	12.5	16.4	9.0
13	12/14/72	?	2150	16.00	3648	10.75	13.1	16.4	9.0
14	10/1/75	?	2003	20.00	3648	16.00	13.0	16.2	12.0
15	3/15/76	?	830	20.00	3648	13.375	12.0	16.2	9.0

To validate the hypothesis that mean values of FPF are not significantly different, a statistical analysis of the data was performed; the results are presented in Table 13. Confidence intervals for the flowing and non-flowing wells are almost the same. The difference between the average FPF values for flowing and non-flowing wells is not significant. Thus, FPF appears not to be a sufficient criterion for identifying risk of flow after cementing.

Table 12. Flow Potential Factor for 30 Wells in GOM.

Flowing Wells		Non-Flowing Wells
Time-to-surface after placement hrs	FPF d-less	FPF d-less
?	0.9	3.4
?	4.5	2
?	2.6	2.8
5.5	4.1	1.7
10.5	1.2	1.9
3.5	3.1	1.9
?	2.2	3.3
?	1.0	2.7
5.5	3.8	1.8
2.3	2.8	1
?	3.0	3.3
8.0	2.7	3
7.0	1.5	3.7
6.0	4.3	3
2.5	3.5	
5.5	4.7	
5.6	**2.9**	**2.7**

Table 13. Statistical Analysis of the FPF's for Flowing and Non-Flowing Wells.

Flowing Wells	
Mean	2.9
Standard Deviation	1.2
Confidence Level (95%)	0.6
95% Confidence Interval	2.3 to 3.5

Non-Flowing Wells	
Mean	2.7
Standard Deviation	1.0
Confidence Level (95%)	0.6
95% Confidence Interval	2.1 to 3.3

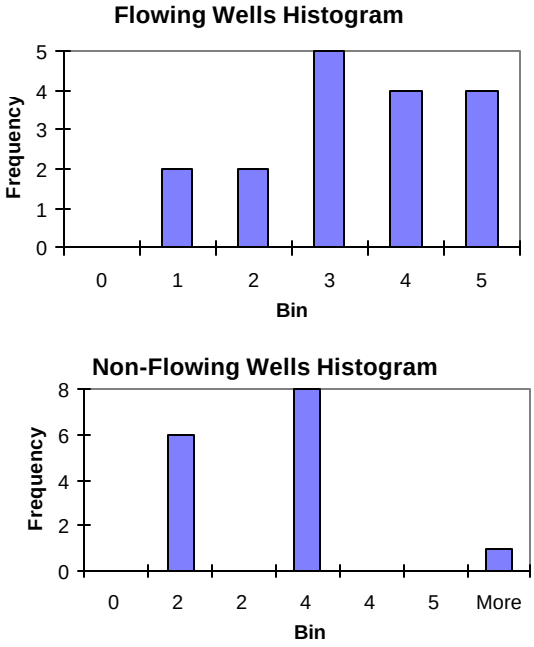

5.3 Time-to-Underbalance Method

A new method for estimating gas flow hazard is proposed and evaluated in this section of the project. In the method, a mathematical model of pressure reduction in the cement column after slurry placement is used to calculate the time when pressure in annulus equals formation pressure of the gas zone; time-to-underbalance (TTU). TTU may be used to qualify risk of gas flow; The shorter the TTU value the higher the risk of gas flow. Since the calculation is performed prior to cementing the well, the slurry can be re-design to assure that no gas migration is possible at TTU.

The time-to-underbalance method seems superior to the FPF method because it does not rely on the arbitrary value of SGS for gas invasion into the slurry, 500 lbf/100 sq.ft. Also, the method draws from a simple reasoning that short TTU leads to early gas invasion into the slurry - hence early appearance of gas on surface, given the same depth. Finally, the method does not use cement properties only but also considers well properties such as depth pressure gradient of the expected high pressure zone.

The utility of the TTU method stems from using a simple criterion to make educated judgment on risk of flow after cementing. However, the method should be validated using statistical correlation between the calculated TTU and the recorded times of gas flow appearance on surface from past incidents of flow after cementing.

Objective of this section is to see if there is any relationship between time to gas flow on the surface and time to pressure balance between cement column pressure and gas formation pressure. In the study, we used two mathematical models of hydrostatic pressure loss in cemented column: the slurry gellation model, and the pressure unloading (transient) model.

5.3.1 Slurry Gellation Model

The model used for the analysis is based on the pressure loss equation due to SGS development: eq. (7B). The effect of filtration and chemical shrinkage on pressure behavior is taken into account by introducing two coefficients: $\zeta(z)$ and $\xi(t)$ into equation (7A) in Section 3:

$$dP = \rho \cdot g \cdot dz - \frac{4 \cdot \tau(\varepsilon)}{D_h - D_c} dz \quad \text{.....(7A)}$$

The equation has been modified as follows:

$$P_h(z,t) = P_{hi} - \xi(t) \cdot \zeta(z) \cdot \frac{4 \cdot SGS(z,t)}{D_h - D_o} \cdot z \quad \text{..... (31)}$$

The coefficient ξ=f(t) is computed by taking first derivatives from the plots of filtration vs. time and cement slurry volume reduction vs. time. Data for the plots were found in the literature: Sutton & Sabins (1990), Sutton & Ravi (1989). Derivatives were computed after the best curve fit had been found for the plots: see Fig. 19 and 20.

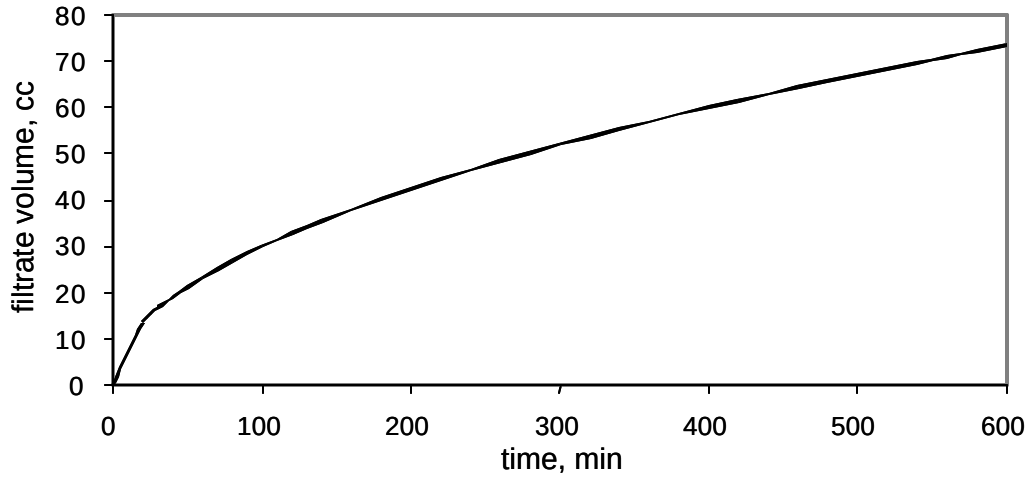

Fig. 19 Cement Class H water loss with fluid loss additive (Sutton & Ravi,1989)

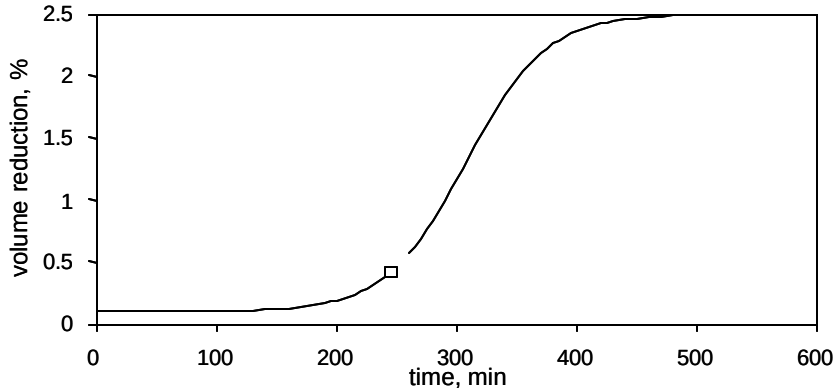

Fig. 20 Shrinkage of Class H cement slurry with fluid loss additive (Sutton & Sabins, 1990)

The premise behind taking derivatives is that the rate of change for both fluid loss and volume reduction due to the chemical reactions are responsible for increasing the shearing rate to which the cement column is subjected. This shearing rate, in turn, causes shear stress within the cement body to appear and hinder hydrostatic pressure transmission. As mentioned before, the strain

must be high enough for shear stress to attain the SGS value, which is the maximum "static" value.

The coefficient ξ is computed by summing up the derivative of fluid loss and volume reduction with respect to time. Both mechanisms are given weights to reflect the importance of each. In this model, volume reduction was given 5 times less weight than fluid loss because the average volume reduction due to filtration was found to be about 17%, which is the mean average from Table 14, while final volume reduction due to chemical reactions can be estimated at 3.5%: see Fig 20. Finally, coefficient ξ is normalized so that the maximum ξ is equal to 1 and corresponds to the most disadvantageous conditions.

The effect of temperature was taken into account by introducing a depth dependent coefficient ζ (z). The maximum value of this coefficient never exceeds 1.5 (1 is for the surface), which means that we assume that at the bottom of the well SGS develops about 50% faster than on the surface. This is in line with cementing schedules according to which cement sets about 50% times faster at 4000 ft than on the surface. By introducing coefficients ξ and ζ, we can introduce both the depth-induced temperature effect and the approximate effect of volume reduction due to fluid loss and chemical reactions into the pressure loss equation. Of course, this is not the correct way they should be incorporated. However, due to the lack of any geological information and cement type for the case histories, we cannot take these phenomena into account in a more accurate way.

Table 14. Hydrostatic Pressure Loss in GOM Wells - Slurry Gellation Model

temperature	depth	initial	pore	time, min									
effect		hydrostatic	pressure	80	90	100	110	120	130	140	150	160	170
coefficient		pressure		gel strength,									
d'less	ft	psi	psi	lbf per 100 sq. ft									
				73	90	116	154	208	285	390	529	711	943
1.1	800	511	391	500	497	493	485	473	454	423	~~376~~	305	202
1.1	900	582	440	569	566	561	553	539	517	482	~~429~~	348	231
1.1	1000	653	489	639	635	629	620	605	580	541	~~481~~	390	260
1.1	1100	723	538	708	704	698	687	670	643	600	~~533~~	433	288
1.1	1200	794	587	777	773	766	754	736	706	658	~~585~~	475	315
1.1	1300	865	635	846	841	834	821	801	768	717	636	~~516~~	342
1.1	1400	935	684	915	910	902	888	866	831	775	688	~~557~~	368
1.1	1600	1077	782	1053	1048	1038	1022	997	956	890	790	~~638~~	419
1.2	1800	1218	880	1192	1185	1174	1156	1127	1080	1005	890	~~717~~	467
1.2	2000	1360	978	1330	1322	1310	1289	1257	1204	1120	990	~~795~~	513
1.2	2200	1501	1075	1468	1459	1445	1423	1386	1327	1234	1089	~~871~~	557
1.2	2400	1643	1173	1605	1596	1581	1556	1515	1450	1347	1186	~~946~~	598
1.2	2600	1784	1271	1743	1733	1716	1689	1644	1572	1459	1283	~~1019~~	637
1.2	2800	1926	1369	1881	1870	1851	1822	1773	1694	1570	1378	~~1090~~	673
1.3	3000	2067	1466	2018	2006	1987	1954	1901	1816	1681	1473	~~1159~~	707
1.3	3200	2208	1564	2156	2143	2121	2086	2029	1937	1792	1566	~~1227~~	738
1.3	3400	2350	1662	2293	2279	2256	2218	2157	2058	1901	~~1658~~	1294	767
1.3	3600	2491	1760	2431	2416	2391	2350	2284	2178	2010	~~1750~~	1359	794
1.3	3800	2633	1857	2568	2552	2525	2482	2411	2298	2118	~~1840~~	1422	818
1.3	4000	2774	1955	2705	2688	2660	2614	2538	2417	2226	~~1929~~	1483	840

Similar tables have been created for all other cases of gas flow from Appendix A (Manowski, 1997). From this information, the time to pressure balance can be seen to vary with depth. It depends strongly on well configuration as well as cement job design. The earliest time to flow predicted by these examples was 150 min., while the flow on the surface has been reported to

occur 10.5 hrs after CIP. Data for all cases are summarized in Table 15. In order to examine if there is a correlation between the time when flow was observed on the surface and the time to earliest pressure balance, plots of the two times have been prepared, as seen in Fig. 21. There is no correlation between the two times both for neat slurry and very weak correlation for retarded slurry.

Table 15. Time-to-Underbalance from Slurry Gellation Model

	Flowing Wells				Non-Flowing Wells
	Flow observed on surface hrs	FPF d'less	Time to earliest pressure balance hrs		Time to earliest pressure balance hrs
			neat slurry	retarded slurry	neat slurry
	?	0.9	2.5	5.0	2.2
	?	4.5	2.5	5.0	2.5
	?	2.6	2.3	4.8	2.7
	5.5	4.1	2.5	5.0	2.5
	10.5	1.2	2.8	7.0	2.7
	3.5	3.1	2.3	4.7	2.7
	?	2.2	2.5	5.3	2.5
	?	1.0	2.5	5.0	2.5
	5.5	3.8	2.7	6.0	2.5
	2.3	2.8	2.5	4.7	2.5
	?	3.0	2.5	5.0	2.5
	8.0	2.7	2.8	7.7	2.5
	7.0	1.5	2.3	4.7	2.3
	6.0	4.3	2.5	5.0	2.3
	2.5	3.5	2.5	5.0	
	5.5	4.7	2.5	5.0	
Average:	5.6	2.9	2.5	5.3	2.5

Two main reasons explain the weak correlations. First, in the slurry gellation model, pressure loss is controlled primarily by the value of SGS. Published SGS curves show a sharp increase in the SGS after about 120 min. in the case of a neat slurry. This increase of SGS is reflected in the model as a sharp decline in the hydrostatic pressure of the cement column at that time. Since there was no other data available to differentiate between the wells, the time when pressures equalize turned out to be roughly the same. The second reason comes from the fact that as mentioned in the section devoted to pressure loss modeling, actual pressure loss is not a function of the SGS only. Actually, the rate of volume reduction will govern the magnitude of pressure loss due to SGS but could not be taken into account in this model correctly since there was no data available on both cement types and geology.

Nevertheless, the study shows that pressure prediction is the preferred type of analysis of flow after cementing. The correlation, though poor, is better than with the FPF and shows promise if more reliable data is made available.

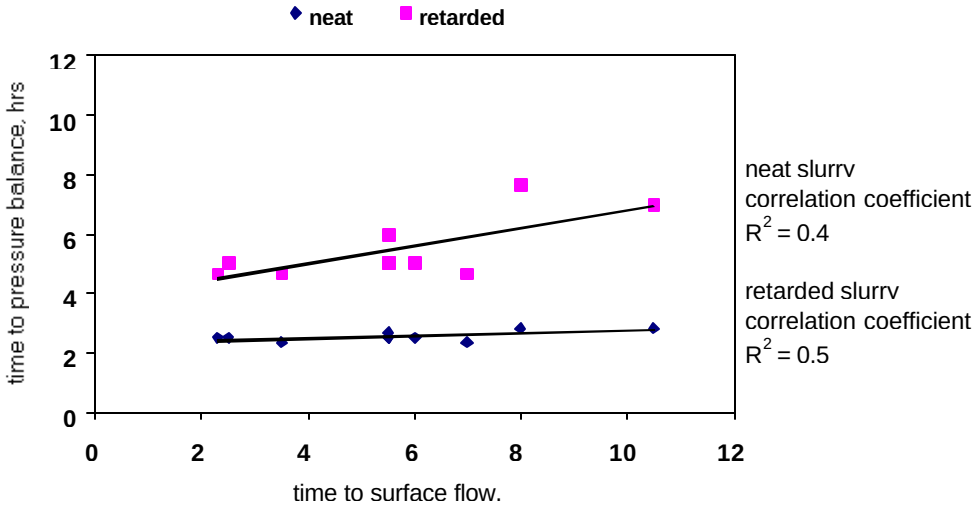

Figure 21. Correlation between time when flow was observed on the surface and calculated time to pressure balance.

5.3.2 Cement Pressure Unloading Model

Using the pressure unloading model (Eq. 17) we calculated hydrostatic pressure loss vs. time and TTU for data from flowing wells in GOM (Appendix A). An example of data for Event 1 is shown in Figure 22, below. Also, the well data is summarized in Tables 16 and 17. Finally, the results of hydrostatic pressure vs. time are shown in Tables 18 - 19 and Fig. 23.

Table 16. Data From Flowing Wells in GOM

Event	Elevation Data		Last CSG					Hole Data			Running Casing								Cement Data			
	ED	WD	OD	ID	Shoe	Pressure Data		Bit	MW	DS	Size	Set Depth					Pressure Data		Lead		Tail	
						Frac.	Pore	Size			OD	ID	MD	TVD	LFC	Frac.	Pore	Volume	WT	Volume	WT
	(ft)	(ft)	(in)	(in)	(ft)	(ppg)	(ppg)	(in)	(ppg)	(dgr.)	(in)	(in)	(ft)	(ft)	(ft)	(ppg)	(ppg)	(cf)	(ppg)	(cf)	(ppg)
1	65	103	30	28.05	322		9	18.5	10	0	13.375	12.515	2698	2698	0		9	0	12.6	2124	15.6
2	85	180	16	15.124	632	10.4EST	9	13.5	9.9	14.8	10.75	9.85	2568	2501	40	12.5	9.2	1030	11.8	348	13.4
3	55	263	20	19	1104	11.2	9	17.5	9.4	0	13.375	12.515	4088	4088	80	15.5	9	4536	12.4	354	15.6
4	105	338	16	15.124	1035		8.3	13.75	10	0	10.75	9.85	2716	2716	40	14.3	10	2016	12.6	236	15.6
5	90	175	16	15.124	800	10EST	9.4	17.5	10	0	13.375	12.515	4707	4707	40	13.8	9.4	0	16.2	4461	16.2
6	36	101	20	19	1000		9	17.5	10	0	13.375	12.515	2000	2000	80		9.5	1950.4	12	520	16.2
7	96	200	20	19	979		9	17.5	9.8	0	13.375	12.515	4000	3500	80		9	3178	12.5	943	16.2
8	110	651	16	15.124	1933	12	9	14.75	11	32	10.75	9.85	4270	4120	80	13.6	9.2		12.6	1575	16.2
9	97	236	20	19	1243	12.8	9	20	11	0	16	15.124	3991	3991	40	14.9	9	3588	11.4	1387	16.2
10	100		18.63	17.755	1335	11	9	17.5	10	45.5	13.375	12.515	4386	4386	80	14.1	9.5	3178	12.6	943	16.2
11	100	70	16	15.124	1000	11.4	9	14.75	9.2	35	10.75	9.85	4045	3940	40	14.4	9	3509	11.7	603	16.4
12	190	90	20	19	1105	10.8	9	17.5	9.2	0	13.375	12.515	4780	4780	40	14.8	9	4211	11.9	2184	16.4
13	161	209	24	23.82	530	11.7	8.4	22	9	23.7	16	15.124	829	826	40	12.2	8.4	1178	12	292	16.2
14	125	194	16	15.124	1013	12	9.5	14.75	11	0	10.75	9.85	4550	4550	60	15.1	9.5	2944	12	650	16.4
15	100	209	20	19	1000	11	9	17.5	9.5	0	13.375	12.515	5462	5462	40	15.3	9.2	5738	11.4	654	16.2
16	99	398	26	24.6	1414	12.3	9	24	11	0	20	19	3326	2236	40	15.5	10.5	3690	12.2	1044	16.4

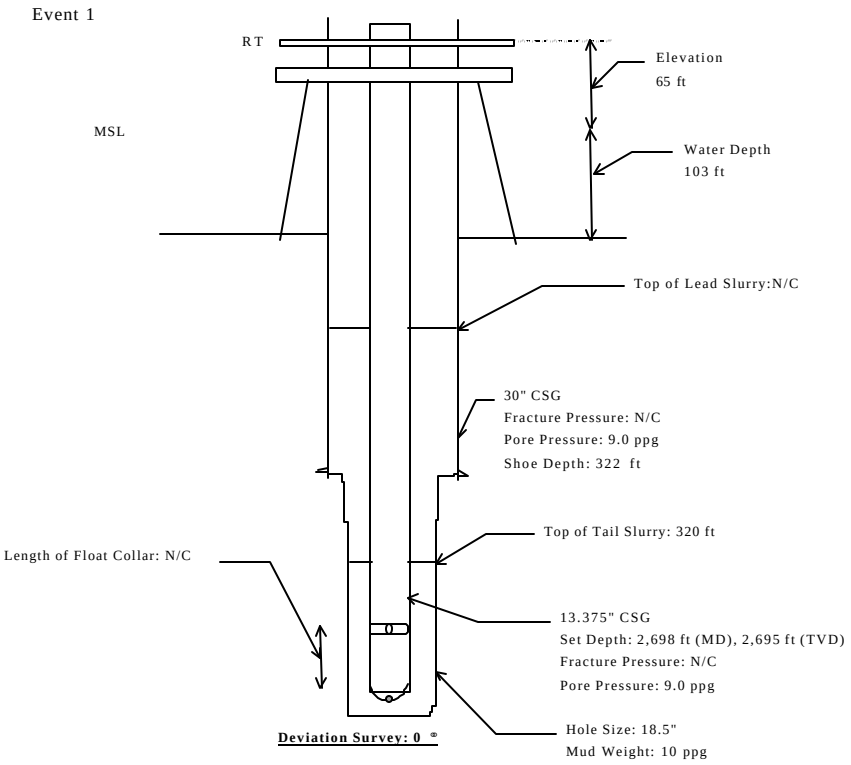

Figure 22. Example of flowing well (Event 1, Appendix A)

Table 17. Hydrostatic Pressure Data from Flowing Wells

Event No.	Average Hole Diameter (in)	Initial Hydrostatic Pressure (psi)	Average Slurry Density (ppg)
1	19.6	2170	15.5
2	13.9	1607	12.4
3	17.9	2704	12.7
4	14.3	1863	13.2
5	17.1	3965	16.2
6	18.3	1390	13.4
7	17.9	2487	13.7
8	14.9	3064	14.3
9	19.7	2791	13.4
10	17.6	3109	13.6
11	14.8	2646	12.9
12	17.8	3683	14.8
13	23.2	558	13.0
14	14.8	3093	13.1
15	17.8	3460	12.2
16	24.4	1566	13.5

Table 18. Calculated Hydrostatic Pressure Loss for Events 1 - 8

Time (min)	Pressure Loss (psi)							
	Event 1	Event 2	Event 3	Event 4	Event 5	Event 6	Event 7	Event 8
0	2,170	1,607	2,704	1,863	3,965	1,390	2,487	3,064
10	1,637	1,403	2,481	1,603	3,600	1,068	2,187	2,732
30	1,358	1,268	2,321	1,427	3,333	953	1,972	2,490
60	1,275	1,197	2172	1,321	3,072	937	1,801	2,270
120	1,263	1,172	2,018	1,276	2,730	936	1,676	2,055
240	1,263	1,170	1,931	1,271	2,397	936	1,640	1,946
480	1,263	1,170	1,914	1,271	2,229	936	1,638	1,928

Table 19. Calculated Hydrostatic Pressure Loss for Events 9 - 16

Time (min)	Pressure Loss (psi)							
	Event 9	Event 10	Event 11	Event 12	Event 13	Event 14	Event 15	Event 16
0	2,791	3,109	2,646	3,683	558	3,093	3,460	1,566
10	2,566	2,852	2,397	3,367	387	2,853	3,299	1,311
30	2,401	2,665	2,217	3,135	387	2,677	3,181	1,149
60	2,243	2,484	2,057	2,909	387	2,509	3,066	1,072
120	2,055	2,270	1,914	2,621	387	2,314	2,907	1,048
240	1,915	2,108	1,852	2,363	387	2,173	2,724	1,046
480	1,871	2,056	1,844	2,250	387	2,132	2,595	1,049

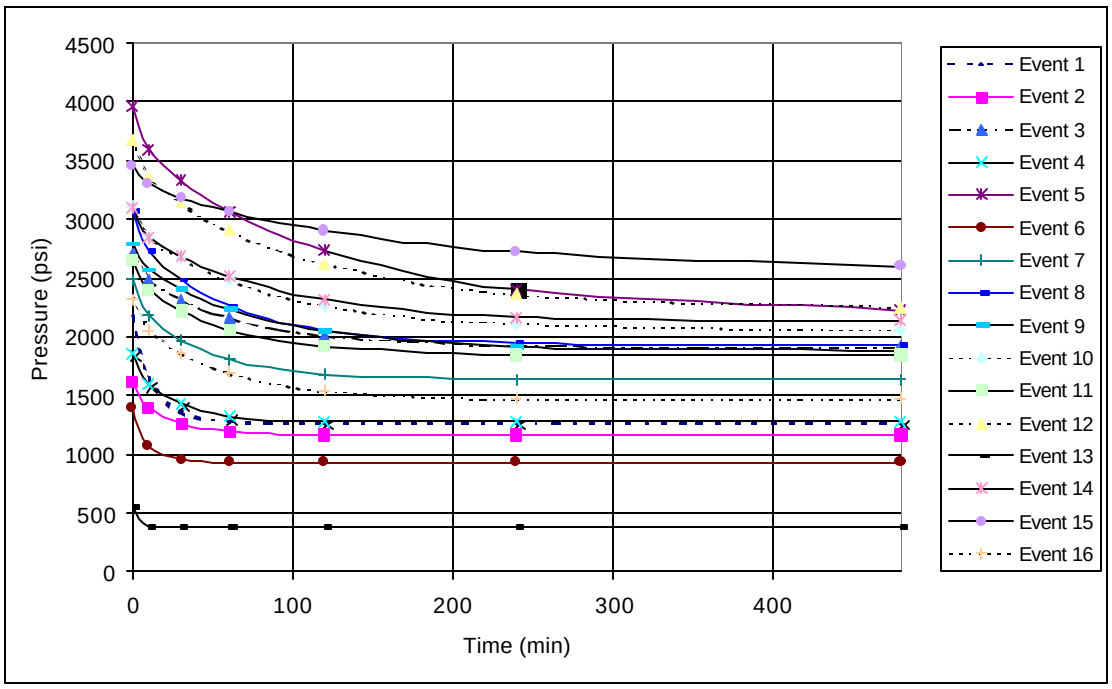

Figure 23. Pressure after cementing in flowing wells in GOM

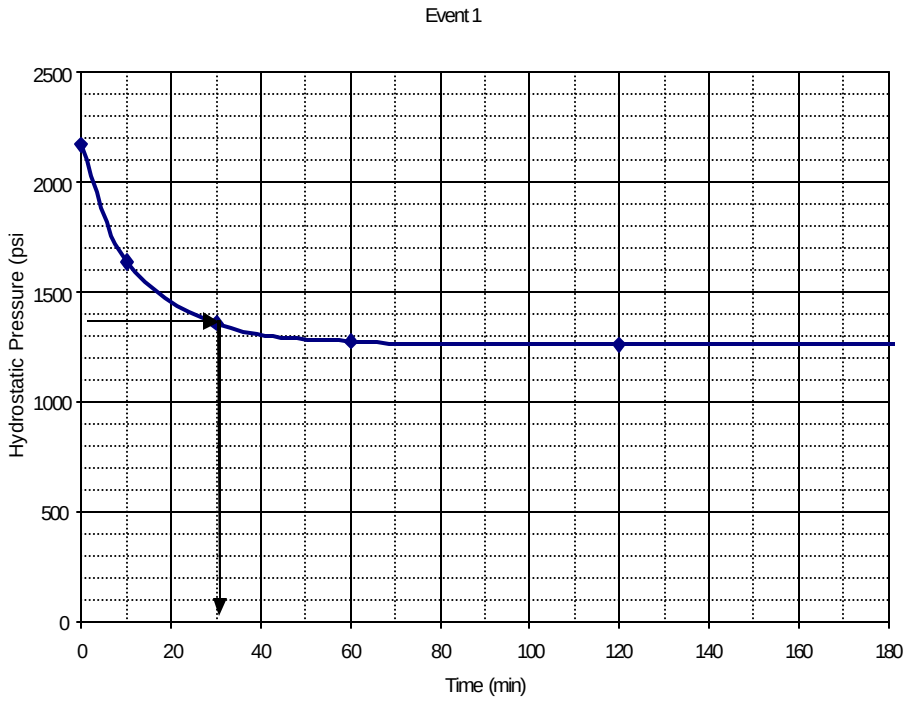

Figure 24. Example of time-to-underbalance calculation

Fig. 24 shows an example of the time-to-underbalance calculations for a single well. Similar plots, shown in Appendix C, have been made for all remaining wells. The calculation procedure was as follows: First, the hydrostatic pressure loss was calculated by Eq. (17). Then, the calculated curve was compared to the gas-zone pressure. Mud density before cementing was assumed to have a safety margin of 0.1 ppg. In other words, the gas-zone pressure is 0.1 ppg lower than the drilling mud before cementing.

The pressure at the gas zone was given by

$$P_e = 0.052 \cdot (\rho_m - 0.1) \cdot L \qquad (32)$$

where:
P_e = gas-zone pressure (psi),
ρ_m = mud weight before cementing (ppg),
0.1 = safety margin while drilling, 0.1 (ppg),
L = casing running depth, TVD, (ft).

Table 20. Time-to-Underbalance from Pressure Unloading Model

Event	Date	Rig Type	Area	TTU (hrs)	Recorded Flow (hrs)
1	9/16/65	Platform	SM	0.5	0
2	12/14/72	Platform	SS	0.5	?
3	10/1/75	Drill Ship	EI	2.7	?
4	3/15/76	Platform	EI	0.6	5.5

5	7/6/77	Drill Ship	SM	3.7	10.5
6	2/14/78	Jackup	MI	0.3	3.5
7	6/1/79	Drill Ship	WD	1.2	1.0
8	5/26/83	Jackup	MC	0.8	0
9	10/21/83	Jackup	GI	1.0	5.5
10	1/8/89	Jackup	MP	2.0	2.3
11	5/8/91	Jackup	BA	2.7	?
12	11/22/92	Jackup	EI	7.5	8.0
13	2/25/93	Jackup	MP	0.6	7.0
14	4/18/93	Jackup	SS	0.8	6.0
15	3/27/94	Jackup	PN	5.2	2.5
16	7/19/94	Jackup	ST	0.3	5.5

The calculated time-to-underbalance is shown in Table 20. It is evident that the pressure-unloading model is more sensitive to well/slurry properties than the gellation model; TTU values in Table 20 vary much more than these in Table 15. Also, values of TTU from the pressure unloading model are much smaller than those from the slurry gellation model. Moreover, there is no good correlation between TTU and the surface flow time recorded in the field.

This difference between modeled values of TTU can be understood by considering the different mechanisms underlying the two models. Transient propagation of pressure loss due bottomhole filtration and compressibility controls the pressure unloading model. The result is a rapid initial pressure reduction that may quickly eliminate pressure overbalance. On the other hand, the gellation model is solely controlled by SGS development, which gives little initial pressure loss and eliminates pressure overbalance only at later times.

In the real well, the two mechanisms act concurrently; Developing SGS slows down propagation of the unloading pressure transient. In the result, the time value may be within the range of the two values obtained from the two models. Thus, combining the two mechanisms in a single model should result in a better correlation.

6. CONCLUSIONS AND RECOMMENDATIONS

The following conclusions can be drawn based on the study described in this report:

1. In view of limited available data, analysis of field cases of flow after cementing has been limited to qualitative circumstantial observations regarding common features of the affected wells such as:
   - Casing strings were set at shallow depths;
   - Hole sizes were relatively large; and,
   - Cement slurries were displaced to the surface.

   Neither of these features, however, could be considered uniquely associated with gas flow as has been shown by comparing "non-flowing" and "flowing" wells.

2. There is no specific property of cement or well that could be related to the incidents of flow after cementing. Based on available cement data (density, and volume) *it is not possible to identify anomalous properties of cement slurries that would make wells flowing*. In fact, it makes more sense to assume that these cements were typical standard slurries. Also, there is no evidence that BOP/diverter nipple-down operation could be a

factor in the phenomenon. Thus, we conclude that *incidents of flow after cementing are statistical events caused by the presence of shallow gas pockets tapped by the wells*. The pockets may go undetected while drilling the well if their pressure gradients are below equivalent pressure gradients of drilling fluid.

3. As the cement slurry could not cause flow after cementing indexing the risk of flow with characteristic "numbers" based upon slurry properties (Slurry Response Number) cannot provide a predictive tool for the risk assessment.

4. Gas flow risk indexing based upon combination of slurry properties and gas zone pressure, Flow Potential Factor *(FPF), does not correlate with incidents of flow after cementing as has been shown statistically in this report*. Firstly, FPF does not show whether (or not) there is an accidental gas pocket in the well. Secondly, FPF considers maximum pressure reduction (MPR) derived from the SGS development thus ignoring rapid initial pressure loss caused by transient effect of pressure unloading due compressibility of the annular cement.

5. A new mathematical model, developed in this project - cement pressure unloading model, considers initial propagation of pressure transient upwards the cement column from the depth of fluid loss into the rock. The model has been validated using data from the field test with pressure gauges installed in the cemented annulus. Bottomhole pressure calculated from the model showed the initial rapid reduction measured in the test well.

6. The pressure unloading model was used in a sensitivity study to identify parameters controlling pressure loss in cement and intrusion of gas, as follows:
    - Large annulus with high water loss would give rapid and large reduction of hydrostatic pressure in the cement column and more likely intrusion of gas;
    - Annular cement system having large compressibility would be more tolerant to fluid loss in terms of losing hydrostatics than the low-compressibility system.

   The first observation implies that surface holes should be more sensitive to gas migration than deep holes. Also, cement slurry filtration should be minimized in surface holes. The second observation emphasizes the importance of determining the annular system compressibility that includes the open-hole lithology. *Further studies are needed to develop practical methods for evaluation of annular compressibility.*

7. A survey of field practices used by operators to control flow-after cementing, performed in this project, shows that the main challenge for operators is to identify area with gas migration problem. Statistical nature if the phenomenon makes operators willing to take a risk rather than to spend money on prevention. Specifically:
    - Operating companies avoid using special cements on a routine basis due to cost; they stress good fluid design, mud displacement and supervision;
    - If a well is drilled in an area known to have given severe problems in the past, special cements are used regularly;
    - Only one operating company uses laboratory tests of gas migration in order to screen various cement compositions for the cementing job.

8. A new predictive tool for gas flow risk assessment has been proposed and evaluated in this project, time-to-underbalance (TTU) method. In the method, theoretical time of hydrostatic pressure reduction down to the gas zone pressure value is calculated and used as a relative estimator of risk; the shorter the TTU value the higher the risk becomes. The method has been statistically validated by seeking a correlation between TTU and actual time of gas flow on the surface recorded in the flowing wells. Two models were used to calculate TTU, cement gellation model (conventional), and the new pressure - unloading model.

   For the gellation model, the correlation was weak mostly due to insensitivity of TTU to the well conditions. As the model is entirely controlled by SGS, and slurries used in the wells were similar calculated TTU gives almost identical values independent from depth.

   For the pressure unloading model the correlation was also weak but the calculated values of TTU were much smaller and varied significantly. Thus, this model should be considered for further work on indexing the gas flow risk assessment.

9. State-of-the-art knowledge and modeling of the pressure loss mechanism in annular cement has been also reviewed in this project. The review shows lack of consistent theory and emphasis on friction (SGS) effect in modeling the pressure loss phenomenon. The effect of cement (annular) compressibility has been considered by some researchers in static rather than dynamic (transient flow) manner.
10. Comparison of TTU values calculated from the gellation and pressure unloading models shows a marked difference: late and early TTU for the gellation and pressure-unloading models, respectively. The difference is extremely important because rapid initial pressure loss indicated by the unloading model may lead to gas migration at very early stage of cement setting when the slurry is still in liquid state. This difference between modeled values of TTU can be understood by considering the different mechanisms underlying the two models. Transient propagation of pressure loss due bottomhole filtration and compressibility controls the pressure-unloading model. The result is a rapid initial pressure reduction that may quickly eliminate pressure overbalance. On the other hand, the gellation model is solely controlled by SGS development, which gives little initial pressure loss and eliminates pressure overbalance only at later times.

    In the real well, the two mechanisms act concurrently; Developing SGS slows down propagation of the unloading pressure transient. In the result, the time value may be within the range of the two values obtained from the two models. Thus, combining the two mechanisms in a single model should result in a better correlation.

The study described in this report leads to the following recommendations regarding field data collection for the purpose of controlling flow after cementing:

1. An analysis of past events using the pressure loss model is dependent upon the quality of input data; in cases in which reliable data cannot be obtained, the resulting model may be only of qualitative value.
2. A need for establishing good databases of all cementing jobs offshore exists; it is a necessary prerequisite for learning from past incidents.
3. Based on the analysis of existing databases of well cementing, a model database storing past incidents of flow should include the following data:

- well location, area, and operator;
- pore pressures and fracturing gradients;
- type of cement used;
- cement density;
- all cement additives used plus their concentration;
- cement properties: SGS and compressibility;
- well configuration;
- wellbore lithology;
- wellbore temperature;
- volume of cement pumped and position of top cement;
- mud type and properties (density changes along the well);
- drilling problems such as kicks, lost returns, annular pressures, etc;
- results of any MWD, LWD and post-job CBL logs.

BIBLIOGRAPHY

Abboud, N.M., and M. Y. Corapcioglu. "Modeling of Compressible Cake Filtration with Sedimentation." *Fluid/Particle Separation Journal* (1997).

Appleby, S. and A. Wilson. "Permeability and Suction in Setting Cement." *Chemical Engineering* Science 51:251-267.

Beris, A.N., J. A. Tsamopoulos, R. C. Armstrong, and R. A. Brown. "Creeping Motion of a Sphere Through a Bingham Plastic." *Journal of Fluid Mechanics* 158 (September 1985).

Bour, D.L., and J. G. Wilkinson. "Combating Gas Migration in the Michigan Basin," SPE Paper presented at the SPE Eastern Regional Meeting, Morgantown, WV (1989).

Chenevert, M. E., and J. Liang. "Model for Predicting Wellbore Pressures in Cement Columns," SPE 19521 (1989).

Cheung, P. R., and R. M. Beirute. "Gas Flow in Cements," SPE 11207 (1982).

Cooke, C. E. Jr., M. P. Kluck, and R. Medrano. "Annular Pressure and Temperature Measurements Diagnose Cementing Operations," IADC/SPE 11416 (1983).

Daccord, G., J. De Rozieres, and B. Boussouira. "Cement Slurry Behavior During Hydration and Consequences for Oil-Well Cementing," Hydration and Setting of Cements RILEM Workshop, Universite de Bourgogne, France, July 3-5, 1991.

Dzuy, N. Q. and D. V. Boger. "Direct Yield Stress Measurement with the Vane Method." *Journal of Rheology* 29(3):335-347.

Garcia, J. A. and C. R. Clark. “An Investigation of Annular Gas Flow Following Cementing Operations,” SPE 5701 (1976).

Haberman, J. P., M. Delestatius, D. G. Hines, G. Daccord, and J.-F. Baret. “Downhole Fluid Loss Measurements from Drilling Fluid and Cement Slurries,” SPE 22552 (1992).

Haimoni, A., and D. J. Hannant. “Developments in the Shear Vane Test to Measure the Gel Strength of Oil Well Cement Slurry.” *Advances in Cement Research* 1(4).

Hanks, R. W., and D. R. Pratt. “On the Flow of Bingham Plastic Slurries in Pipes and Between Parallel Plates,” SPE 1682 (1967).

Harris, K.L., K. M. Ravi, D. S. King, J. G. Wilkinson, R. R. Faul. “Verification of Slurry Response Number Evaluation Method for Gas Migration Control,” SPE 20450 (1990).

Hartog, J. J., D. R. Davies, and R. B. Stewart. “An Integrated Approach for Successful Primary Cementations.” *JPT*, September 1983.

Manowski , W. “Design Method for Top Cement Pulsation to Prevent Flow after Cementing.” Master’s Thesis, Louisiana State University (1997).

Marlow, Roy S. “Cement Bonding Characteristics in Gas Wells,” *JPT* (November 1989).

Meeten, G. H. and J. D. Sherwood. “Vane Technique for Shear-Sensitive and Wall-Slipping Fluids,” *Theoretical and Applied Rheology* (1992).

Nishikawa, S. “Mechanism of Gas Migration after Cement Placement and Control of Sustained Casing Pressure,” Master’s Thesis, Louisiana State University (May 1999).

Prohaska, M., R. Fruhwirth, and M. J. Economides. “Modeling Early-Time Gas Migration Through Cement Slurries.” *SPE Drilling and Completion* (September 1995).

Prohaska, M., D. O. Ogbe, and M. J. Economides. “Determining Wellbore Pressures in Cement Slurry Columns,” SPE 26070 (1993).

Rae, P., D. Wilkins, and D. Free. “A New Approach to the Prediction of Gas Flow after Cementing,” SPE 18622 (1989).

Sabins, Fred L., John M. Tinsley, and David L. Sutton. “Transition Time of Cement Slurries between the Fluid and Set State,” SPE 9285 (1980).

Sabins, Fred, and Michael L. Wiggins. “Parametric Study of Gas Entry into Cemented Wellbores,” SPE 28472 (1994).

Stewart, R. B., and F. C. Schouten. “Gas Invasion and Migration in Cemented Annuli: Causes and Cures,” SPE 14779 (1986).

Sutton, D. L., and K. M. Ravi. “New Method for Determining Downhole Properties that Affect Gas Migration and Annular Sealing,” SPE 19520 (1989).

Sutton, D. L., and F. L. Sabins. “Interrelationship Between Critical Cement Properties and Volume Changes During Cement Setting,” SPE 20451 (1990).

Webster, W. W., and J. V. Eikerts. “Flow After Cementing: A Field and Laboratory Study,” SPE 8259 (1979).

APPENDIX A:
FIELD CASES OF FLOW AFTER CEMENTING IN GOM

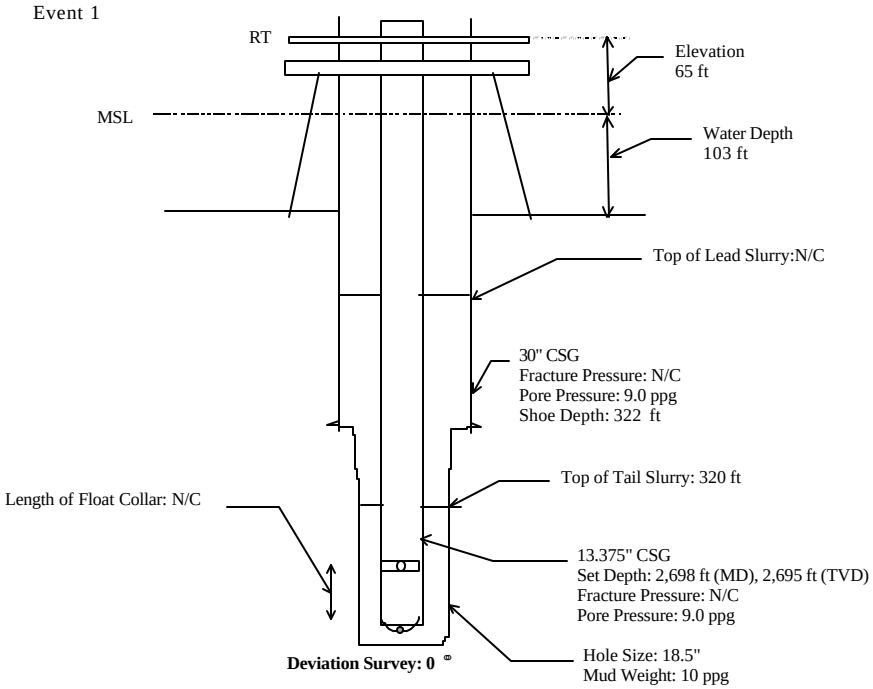

Fig.A.1 Event 1

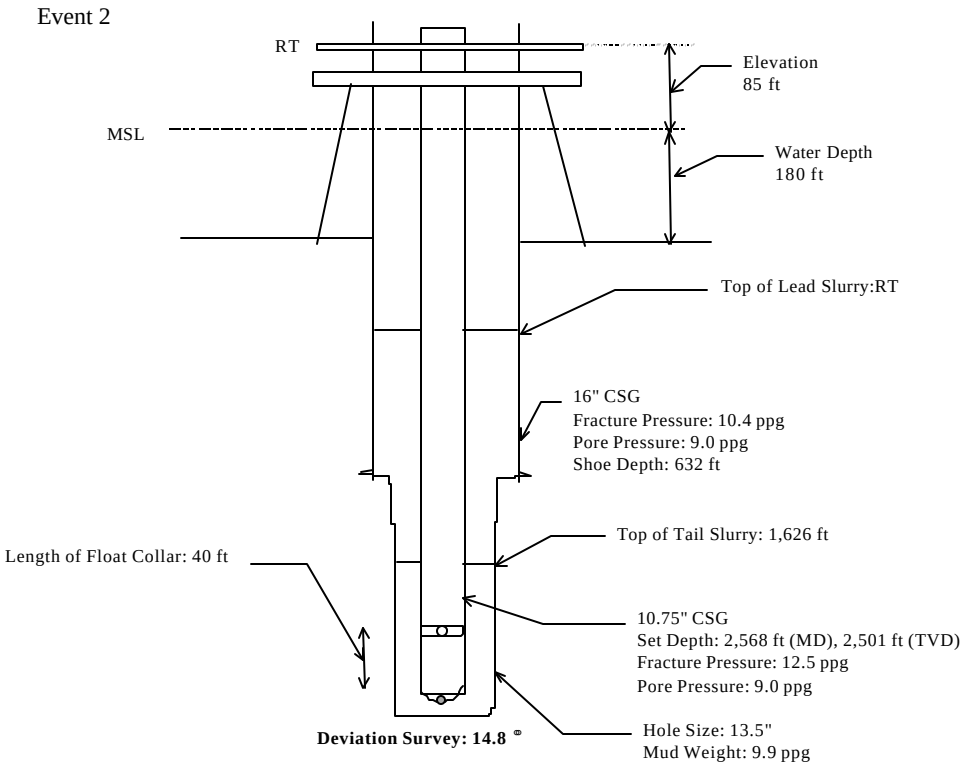

Fig.A.2 Event 2

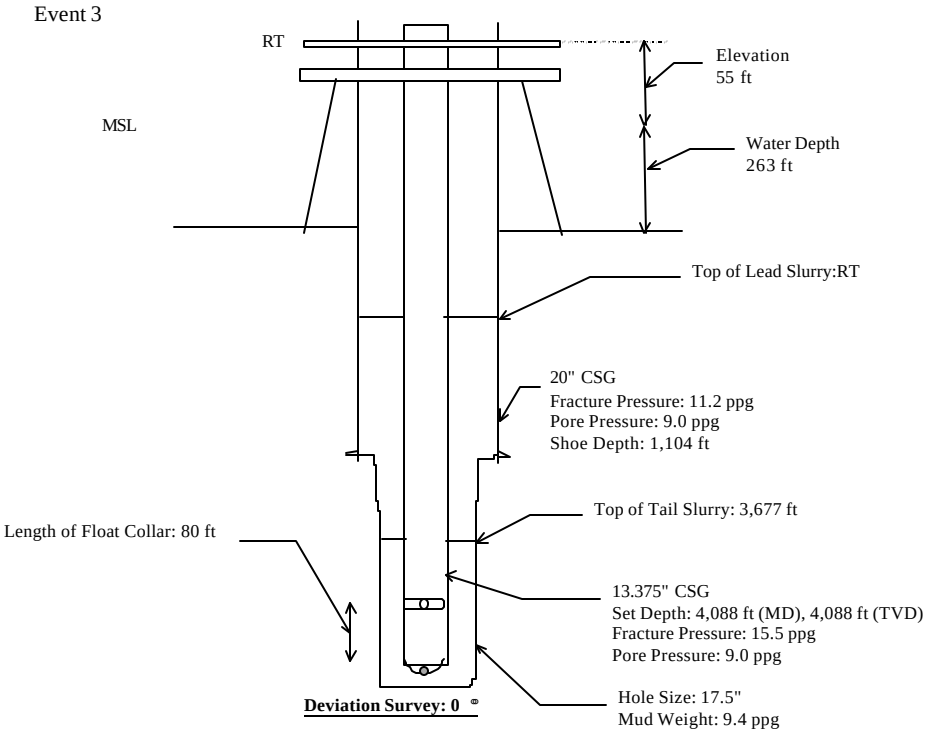

Fig.A.3 Event 3

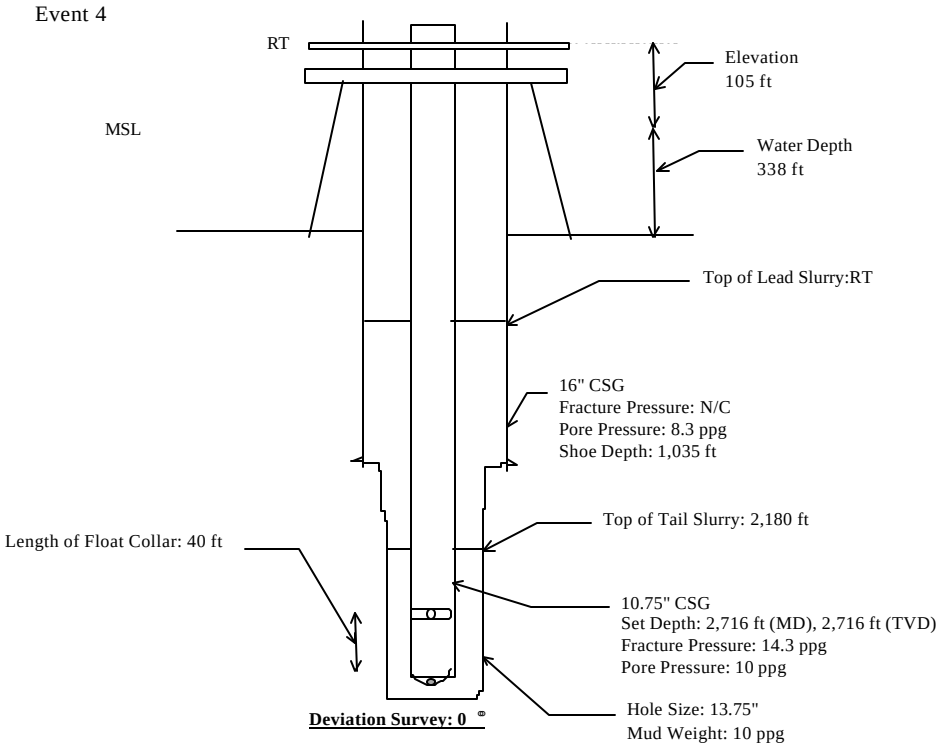

Fig.A.4 Event 4

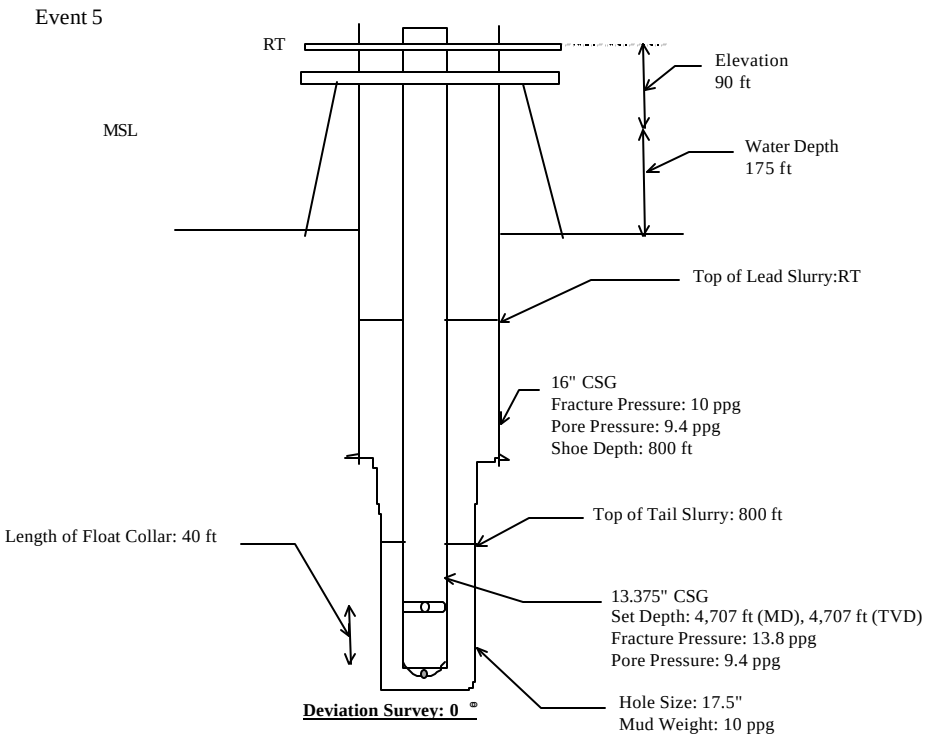

Fig.A.5 Event 5

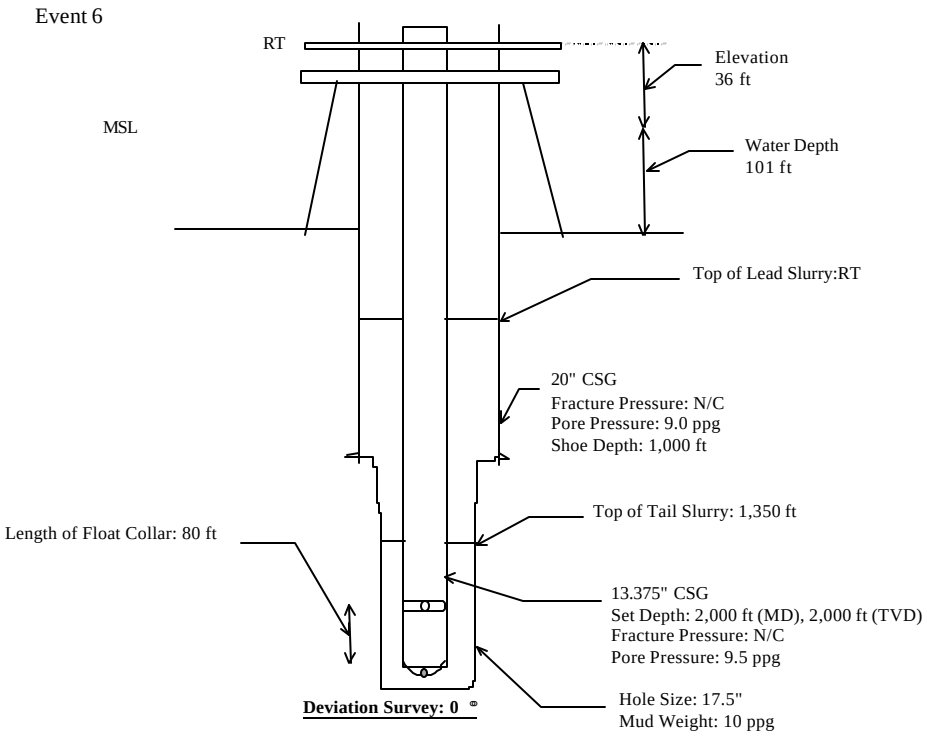

Fig.A.6 Event 6

Event 7

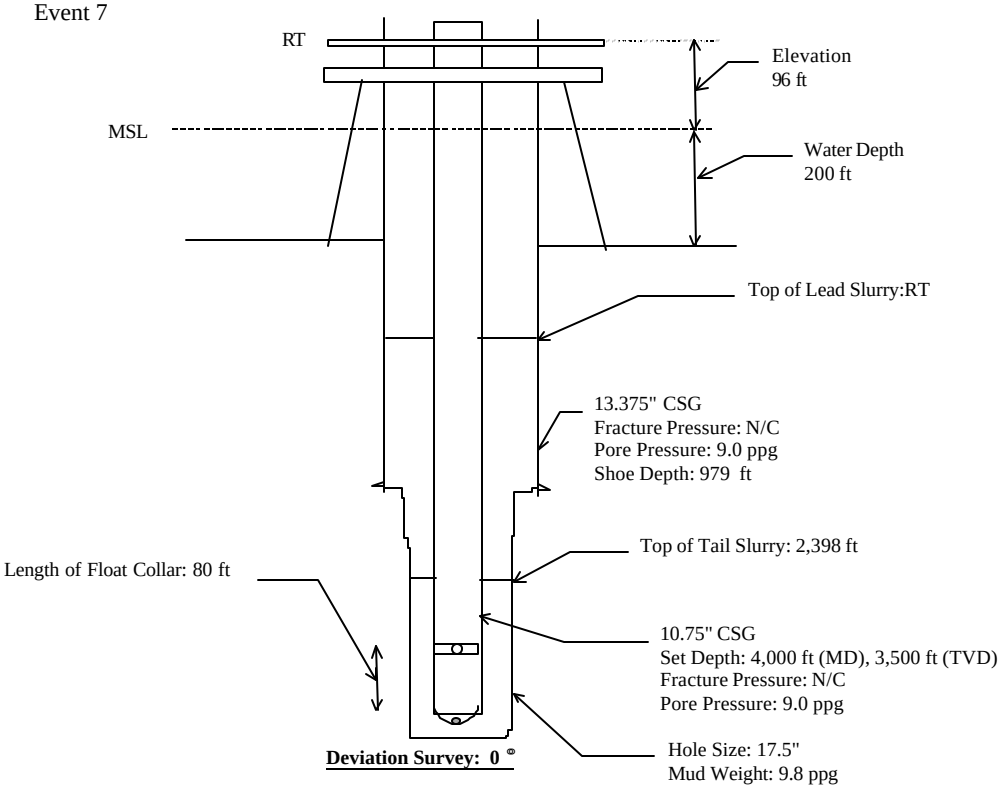

Fig.A.7 Event 7

Event 8

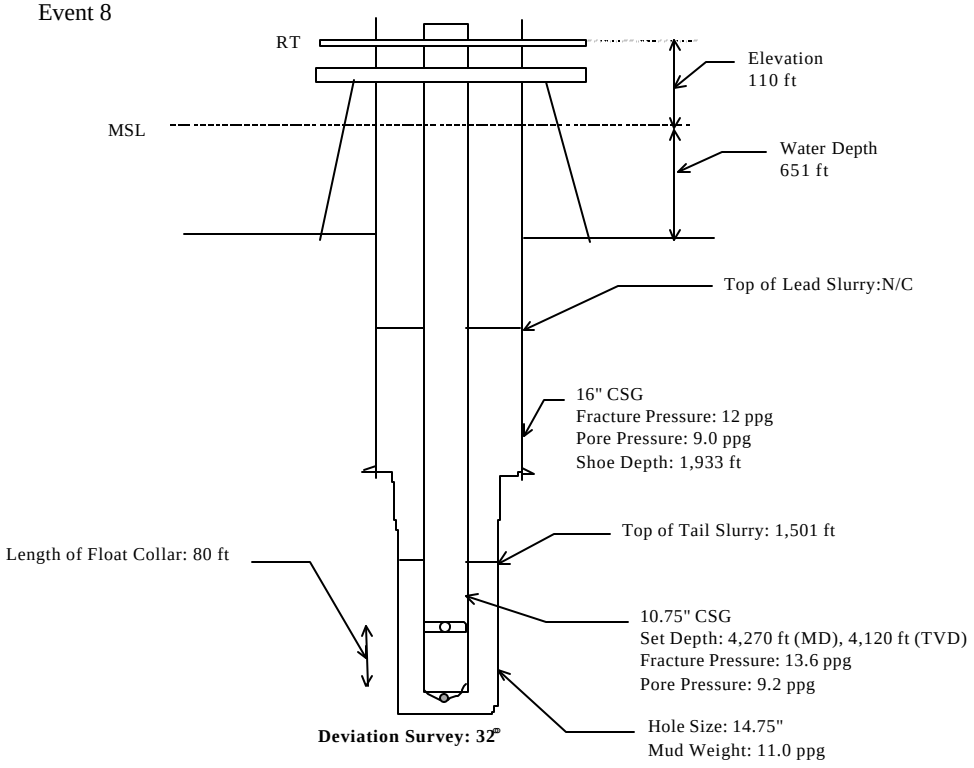

Fig.A.8 Event 8

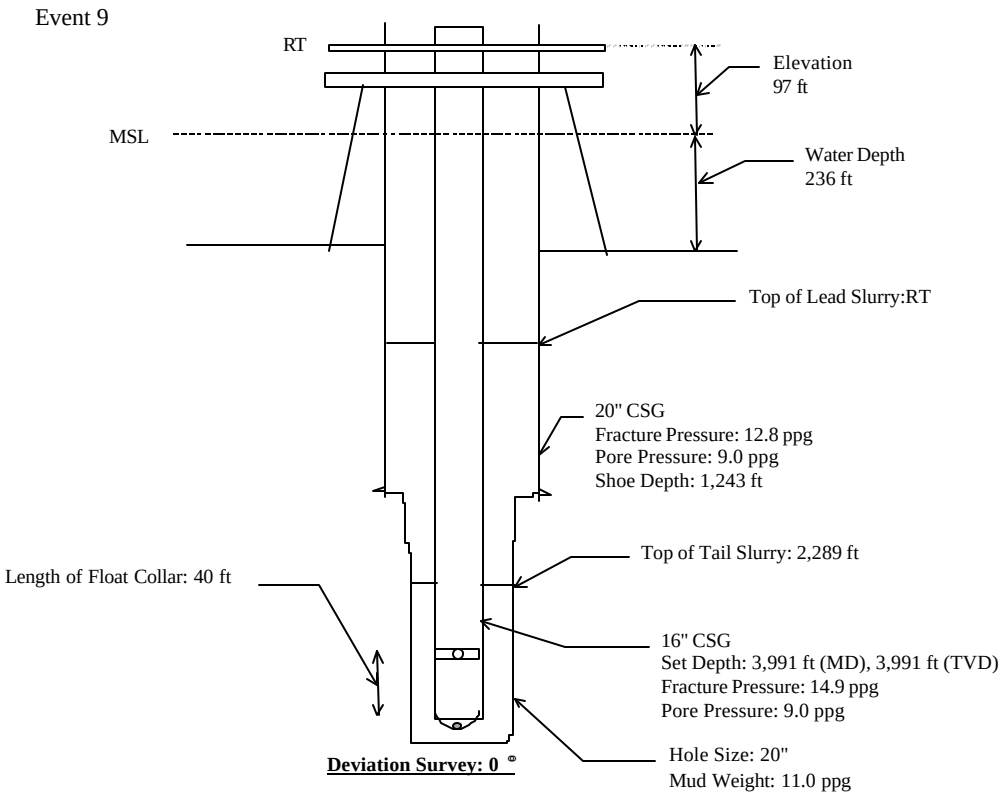

Fig.A.9 Event 9

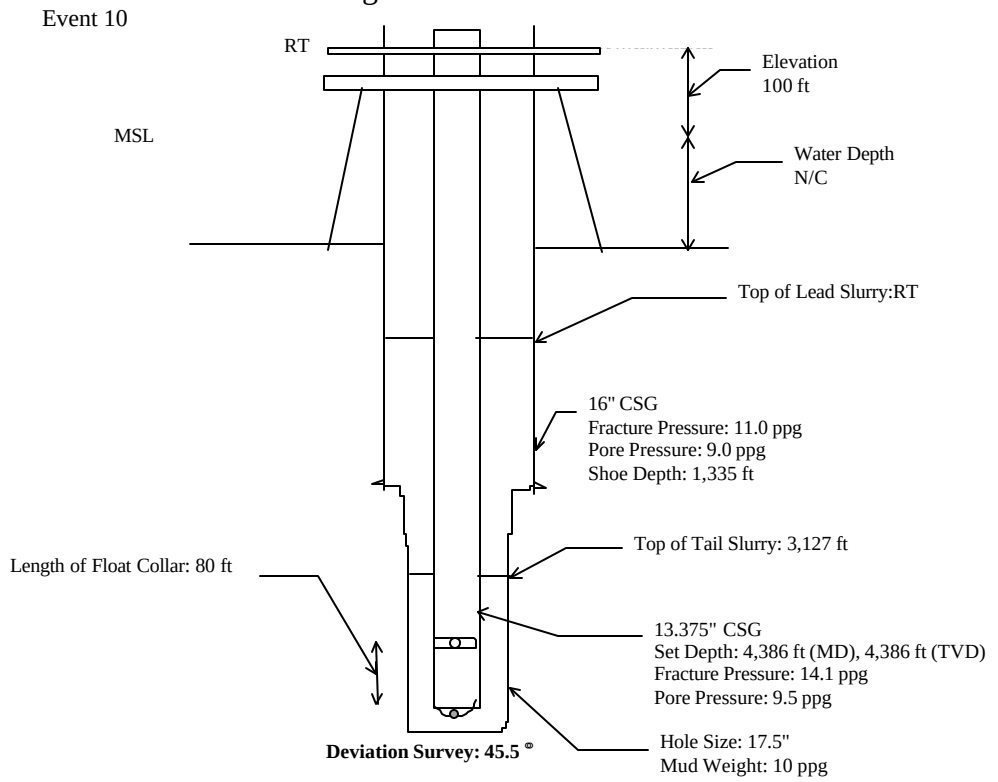

Fig.A.10 Event 10

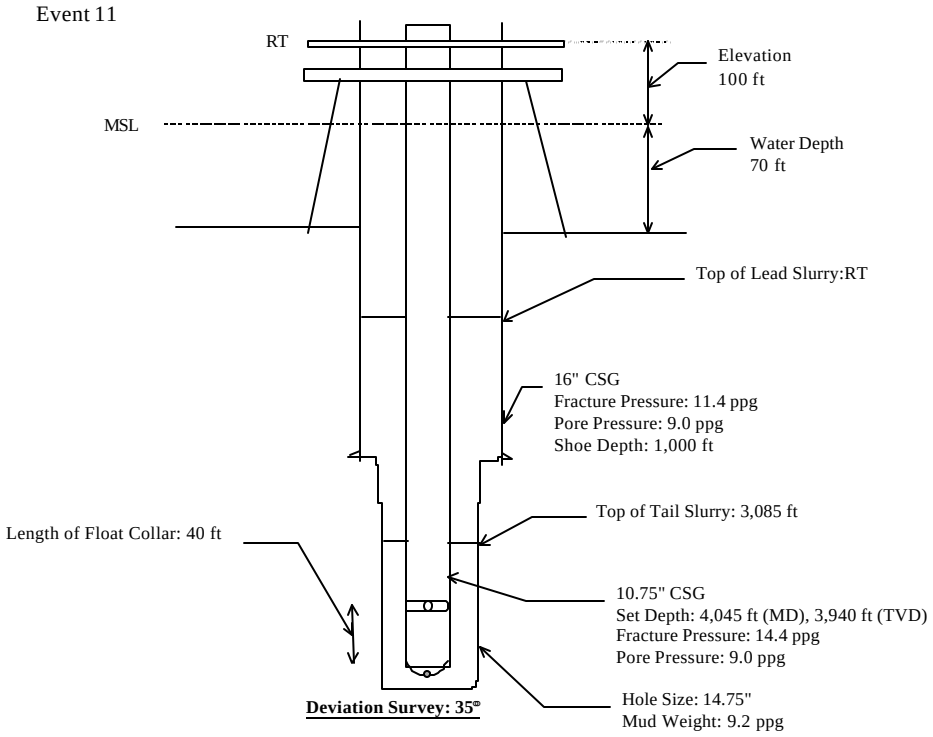

Fig.A.11 Event 11

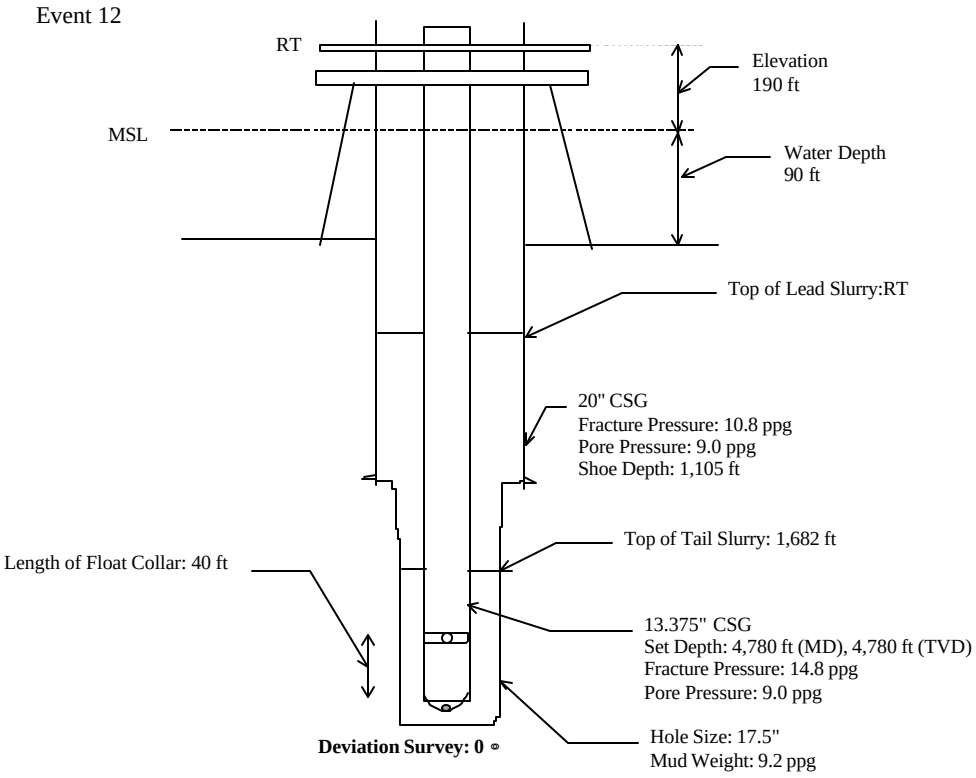

Fig.A.12 Event 12

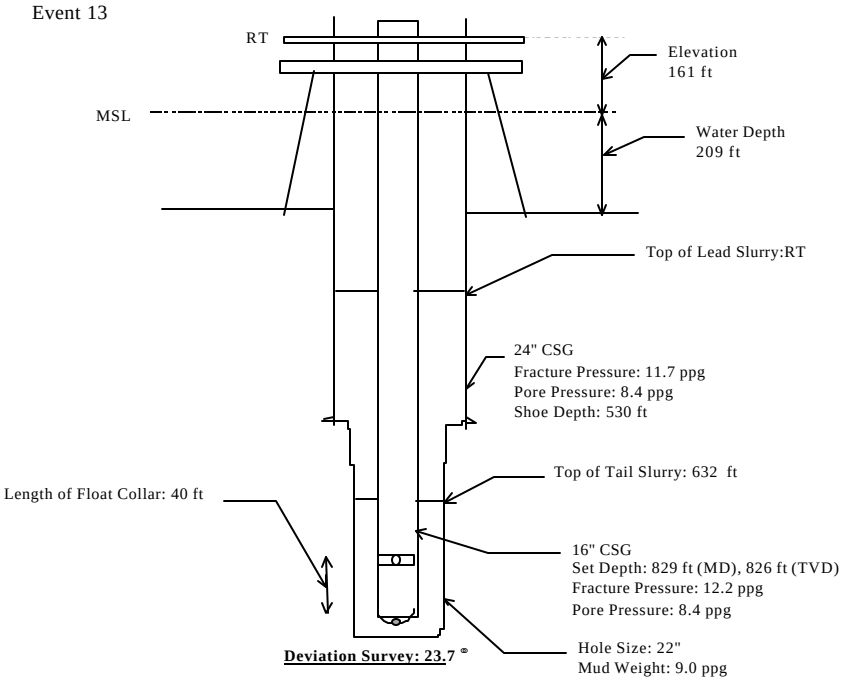

Fig.A.13 Event 13

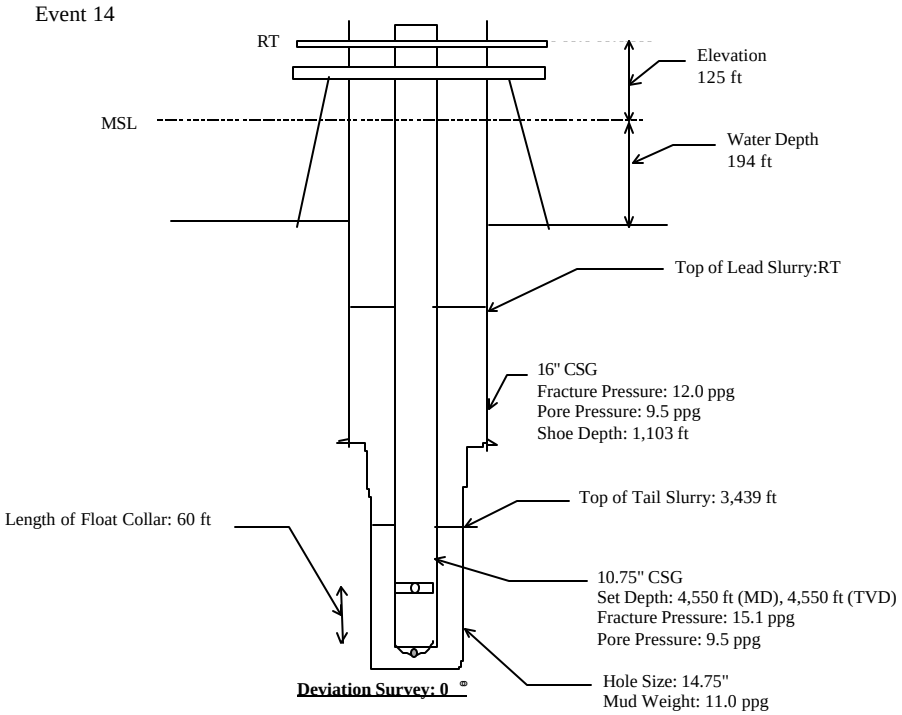

Fig.A.14 Event 14

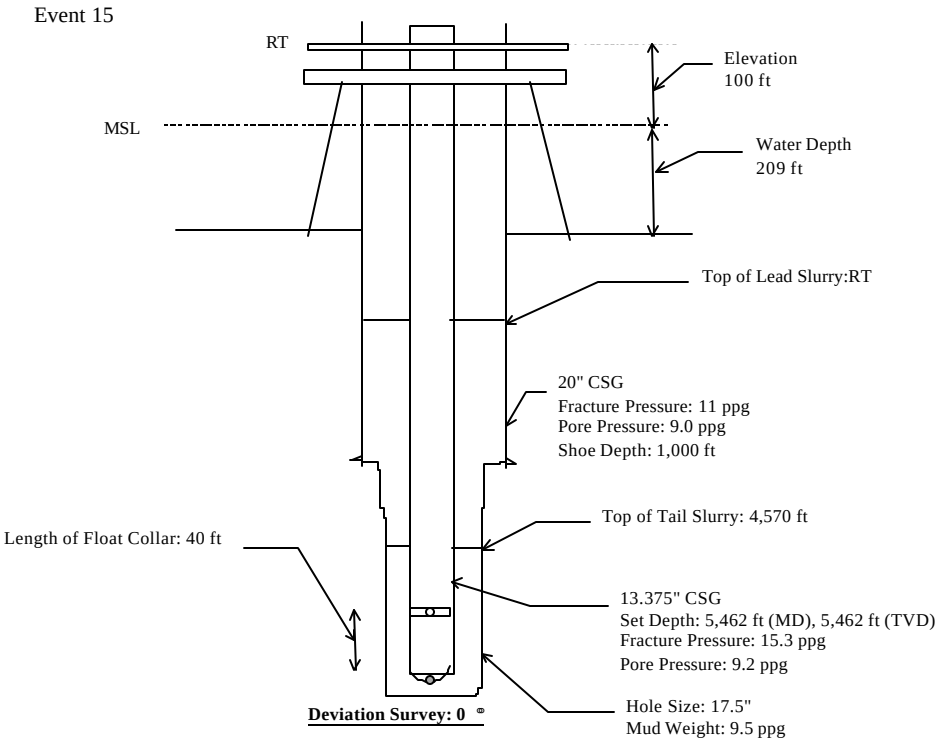

Fig. A.15 Event 15

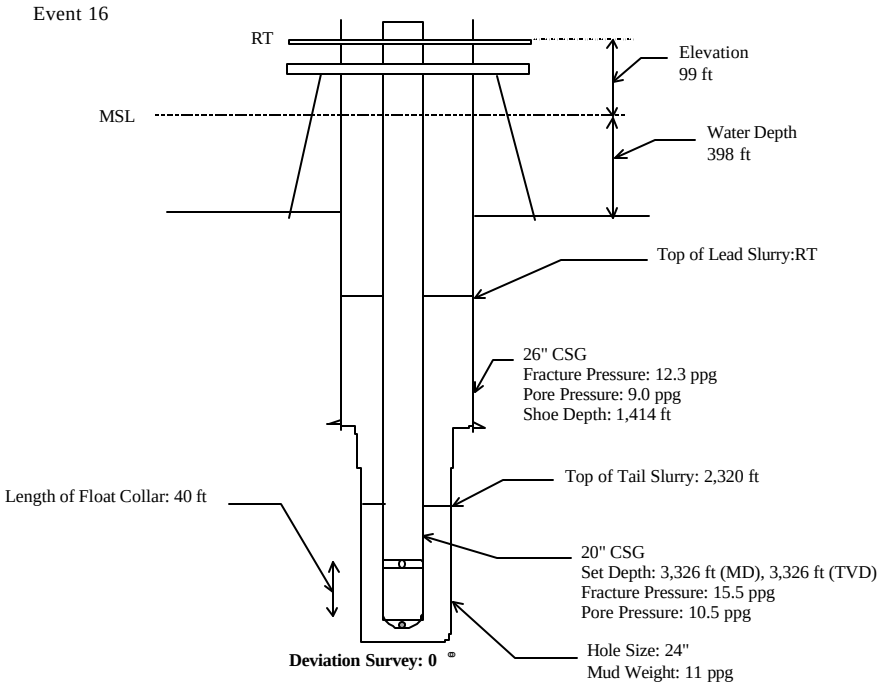

Fig. A.16 Event 16

APPENDIX B:

TECHNIQUES AND PROCEDURES TO PREVENT FLOW AFTER CEMENTING IN GOM

Operator:	Special cements used:	Other techniques / operations:
BP	• avoid using special cements on routine basis, • use of chemical grouts to plug flowing zones.	• emphasis on casing centralization and good mud / spacer / cement design, • use of turbulators to spin cement and enhance mud displacement efficiency, • recommend drilling with marine risers and driving casing to 2000 ft below mud line, • introduced contingency plans to tackle the problem.
Shell	• salt-saturated cements, • cement substitutes, • compressible cements, • surfactant cements, • slag mix cements.	• focus on good mud displacement.
Phillips Petroleum	• cements: silica fume, colloidal silica.	
Mobil	• lightweight cements with guar, sugar or polymers to control free water.	
Arco	• latex expanding thixotropic cements	• good supervision of cementing job execution
Texaco	• right angle set cements.	• focus on proper displacement: recommend use of centralizers, • proper design of fluid rheology, filtration and pumping conditions,

		• increasing mud and spacer density above cement column.
Unocal	• right angle set cements, • latex cements, • foamed cements.	• low fluid loss, • zero settling, • proper supervision of job execution, • customized spacers and preflushes to maximize mud displacement.
Amoco	• gas migration test screening,	
Conoco	• cements with quick transition time,	• emphasis on fluid loss control. and avoidance of cement retardation

APPENDIX C

TIME-TO-UNDERBALANCE CALCULATIONS

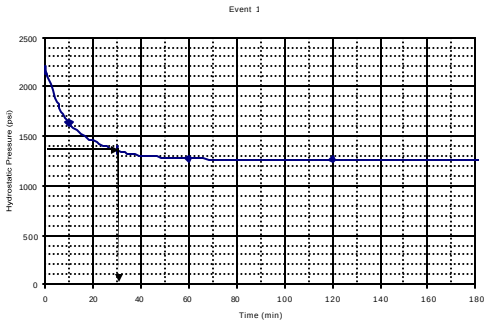

Fig.C.1 Event 1

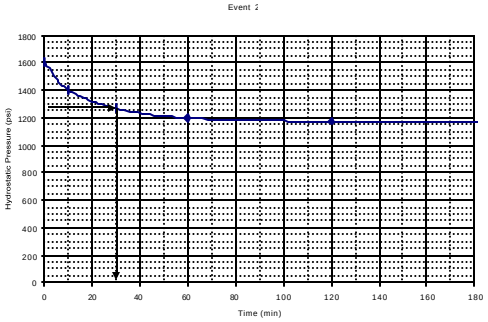

Fig.C.2 Event 2

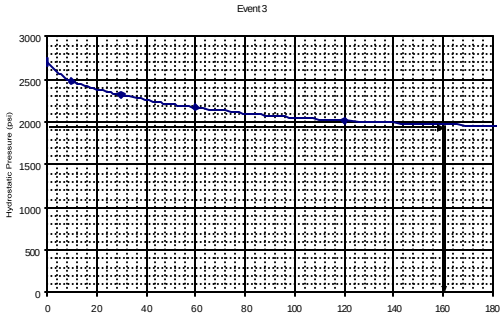

Fig.C.3 Event 3

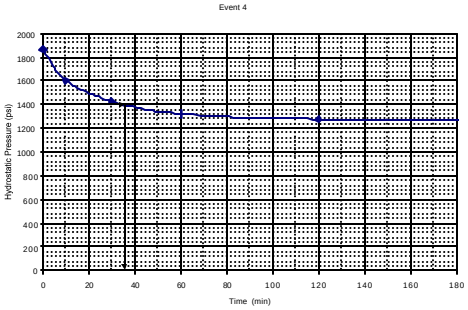

Fig.C.4 Event 4

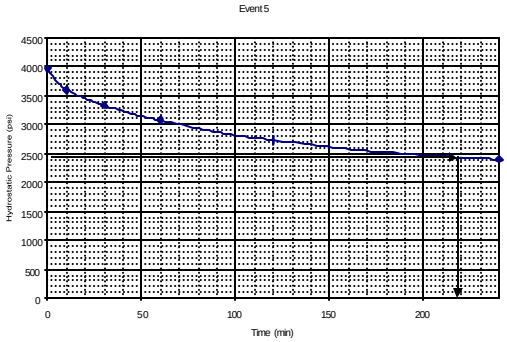

Fig.C.5 Event 5

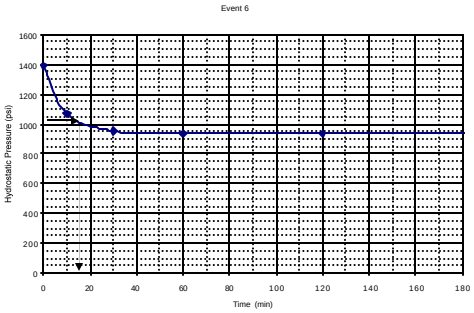

Fig.C.6 Event 6

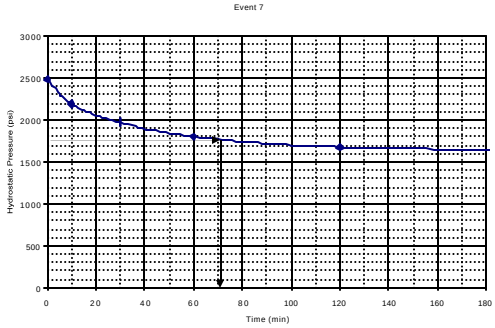

Fig.C.7 Event 7

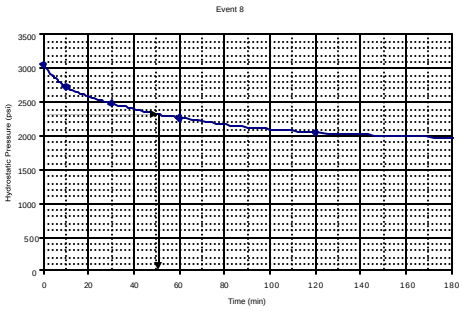

Fig.C.8 Event 8

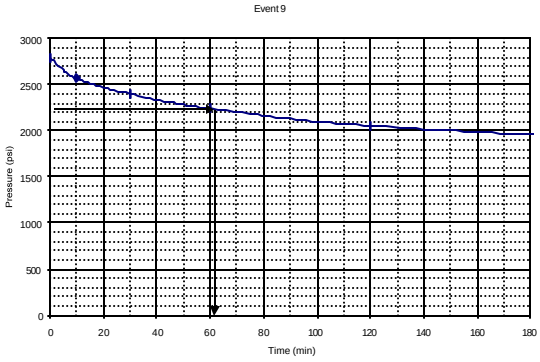

Fig.C.9 Event 9

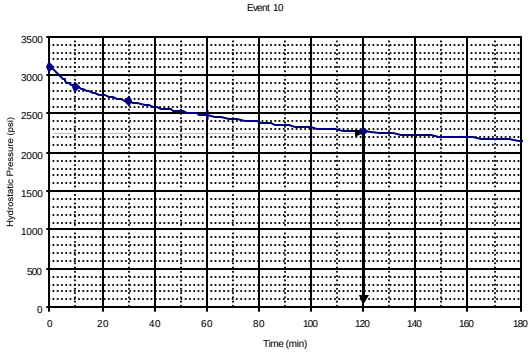

Fig.C.10 Event 10

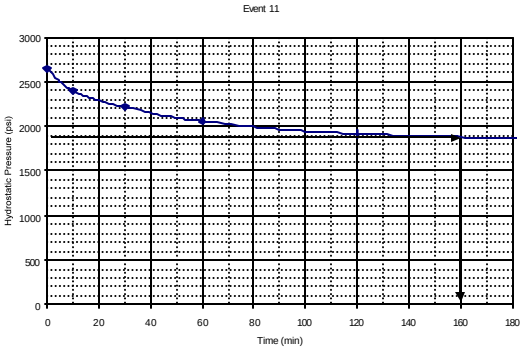

Fig.C.11 Event 11

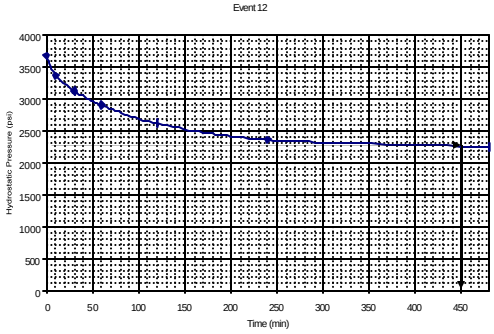

Fig.C.12 Event 12

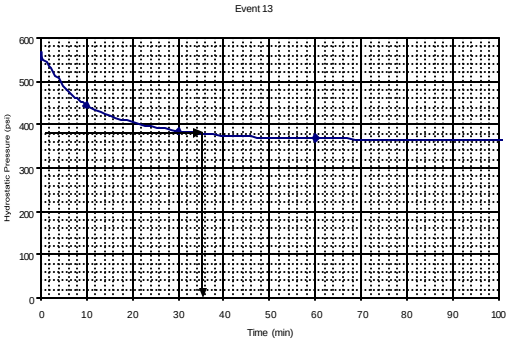

Fig.C.13 Event 13

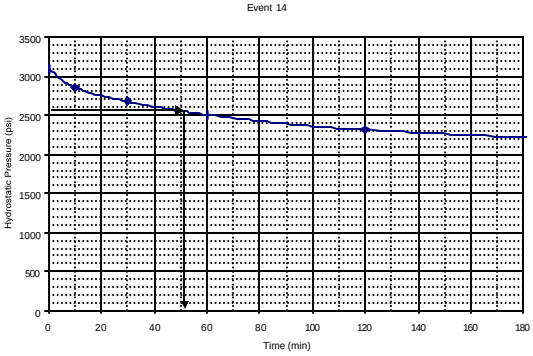

Fig.C.14 Event 14

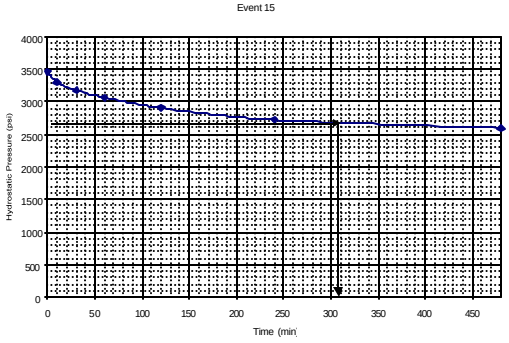

Fig.C.15 Event 15

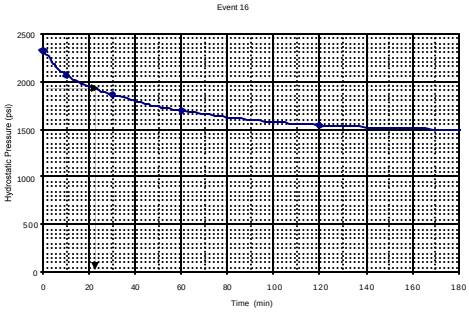

Fig.C.16 Event 16